Water Research 272 (2025) 122938

Contents lists available at ScienceDirect

Water Research

journal homepage: www.elsevier.com/locate/watres

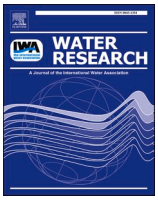

Calcium-organic matter fouling in nanofiltration: Synchrotron-based X-ray fluorescence and absorption near-edge structure spectroscopy for speciation

Tyler A. Malkoske [a], Yang-Hui Cai [a], Sharon E. Bone [b,1], Andrea I. Schäfer [a,*]

[a] Institute for Advanced Membrane Technology (IAMT), Karlsruhe Institute of Technology (KIT), Hermann-von-Helmholtz-Platz 1, 76344 Eggenstein-Leopoldshafen, Germany
[b] Stanford Synchrotron Radiation Laboratory, SLAC National Accelerator Laboratory, Menlo Park, CA 94025, United States

ARTICLE INFO

Keywords:
Physico-chemical water treatment
X-ray spectroscopy
Membrane fouling mechanisms
Scaling
Osmotic backwash

ABSTRACT

Calcium (Ca)-enhanced organic matter (OM) fouling of nanofiltration (NF) membranes leads to reduced flux during desalination and requires frequent cleaning. Fouling mechanisms are not fully understood, which limits the development of targeted fouling control methods. This study employed synchrotron-based X-ray fluorescence (XRF) and X-ray absorption near-edge structure (XANES) spectroscopy to quantify the spatial distribution and mass of Ca deposition as well as changes in the Ca coordination environment characteristic of specific fouling mechanisms, respectively. Bench-scale filtration experiments were performed using feed solutions containing Ca and ten different types of organic matter (OM), as well as the common scalants, calcium carbonate ($CaCO_3$) and calcium sulfate ($CaSO_4$). Osmotic backwash (OB) was performed at regular intervals for fouling control. Ca-OM aggregation resulted in greater flux decline and lower flux recovery during OB than Ca conditioning of membranes followed by filtration of feed solution with OM. Linear combination fitting (LCF) of XANES absorption spectra from fouled membranes indicated that Ca-OM aggregation preferentially occurred for OM types that exhibited both high carboxylic group and negative charge density. Consequently, these OM types exhibited greater deposition of Ca and TOC on the membrane surface when compared to other OM types. For the coexistence of scalants and OM, Ca speciation within the fouling layer was characteristic of both Ca bound to the membrane (i.e. potential bridging, charge screening) as well as Ca-OM aggregation and deposition mechanisms, while a range of crystal polymorphs were observed to occur simultaneously. XRF and XANES represent powerful tools for the elucidation of NF fouling mechanisms by quantification of Ca deposition as well as Ca speciation. Fouling control methods should target OM types with high carboxyl group density and negative charge to neutralize or eliminate interactions with Ca.

1. Introduction

1.1. Brackish water desalination using nanofiltration

Decentralized photovoltaic powered nanofiltration (PV-NF) is a robust technology for the provision of drinking water through brackish water desalination and surface water treatment in off-grid rural areas (Schäfer et al., 2014; Vivar et al., 2024). Membrane fouling by organic matter (OM), which may occur in both groundwater and surface waters, can reduce membrane flux and requires regular cleaning (Rolf et al., 2022; Tong et al., 2023). Some brackish and surface waters contain relatively high concentrations of inorganic scalants, including calcium carbonate ($CaCO_3$) and calcium sulphate ($CaSO_4$), which may contribute to flux decline due to scaling (Greenlee et al., 2009).

1.2. Osmotic backwash for fouling control

When considering batteryless directly coupled PV-NF, osmotic backwash (OB) represents a chemical free cleaning method (Cai et al., 2021). OB occurs during solar irradiance fluctuations when reduced pump speed causes the operating pressure to spontaneously drop below the osmotic pressure of the feed solution, resulting in backflow of water

* Corresponding author.
E-mail address: Andrea.Iris.Schaefer@kit.edu (A.I. Schäfer).
[1] New address: Institute of Bio- and Geosciences Agrosphere (IBG-3), Forschungszentrum, Juelich.

https://doi.org/10.1016/j.watres.2024.122938
Received 19 July 2024; Received in revised form 15 November 2024; Accepted 8 December 2024
Available online 9 December 2024

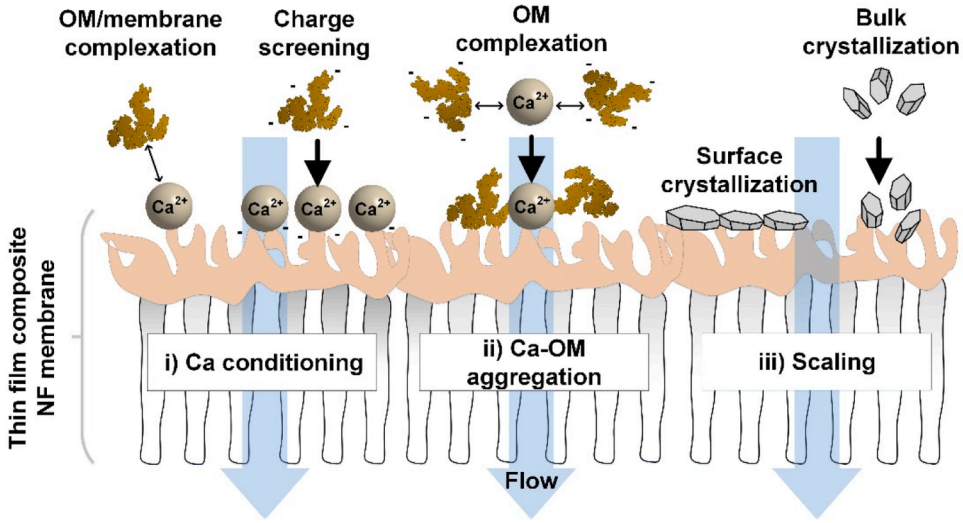

Fig. 1. Major roles of Ca in OM fouling and scaling of NF: i) bridge between OM and membrane surface; ii) deposition of Ca-OM complex; iii) surface/bulk crystallization.

from the permeate side to the feed side of the membrane (Cai and Schäfer 2020, Sagiv and Semiat 2005). OB has been previously utilized for fouling as well as scaling control during desalination at both bench- (Lee et al., 2021) and pilot-scale (Alnumani et al., 2024), while its impact on membrane integrity has been investigated (Cai et al., 2024).

1.3. Nanofiltration fouling and scaling mechanisms

NF fouling and scaling proceed according to mechanisms (Fig. 1) that result in different levels of flux decline. OM fouling includes adsorption and deposition of OM onto the membrane surface (Chon and Cho, 2016; Hong and Elimelech, 1997; Li and Elimelech, 2004; Schäfer et al., 2021). The presence of multivalent cations, in particular calcium (Ca), can enhance OM fouling via: (i) altering membrane surface properties (referred to as 'Ca conditioning' in the present study), in which Ca bound to the membrane surface binds to OM molecules in the bulk solution (Lee et al., 2021; Yoon et al., 1998) or reduces repulsion between negatively charged OM in the bulk solution and the membrane surface by charge screening (Shim et al., 2002), and (ii) Ca-OM aggregation, whereby Ca acts as a bridge between multiple OM molecules, which subsequently deposit onto the membrane surface (Adusei-Gyamfi et al., 2019; Mi and Elimelech, 2008). Scaling occurs when the concentration of sparingly soluble scalants (e.g. $CaCO_3$, $CaSO_4$) exceeds the solubility limit due to concentration polarization (CP) at the membrane surface, leading to (iii) surface or bulk crystallization and the formation of mineral crystals (e.g. calcite, gypsum) (Hong and Elimelech, 1997; Sari and Chellam, 2017; Schäfer et al., 1998; Tang et al., 2007b). Surface crystallization is characterized by heterogeneous nucleation and lateral crystal growth directly on the membrane surface, while bulk crystallization includes homogeneous nucleation in the bulk solution followed by deposition onto the membrane surface (Rolf et al., 2022).

When considering Ca-enhanced OM fouling, it remains unclear which of Ca conditioning or Ca-OM aggregation is the predominant mechanism and the relative contribution of each to NF fouling. Indeed, Ca-enhanced OM fouling mechanisms and NF fouling may vary due to differences in OM type, such as the density of functional groups (e.g. carboxyl, phenol) (Lee and Elimelech, 2006; Park et al., 2018). Neutralization of carboxyl groups present in OM by complexation with Ca reduces repulsion between OM and negatively charged membrane surfaces, thereby enhancing adsorption and membrane fouling (Adusei-Gyamfi et al., 2019). Ca-OM complexation also creates larger 'flocs' with greater drag force towards and smaller back diffusion away from the membrane, increasing deposition (Schäfer et al., 1998). For scalants, the morphology and structure of deposited minerals (e.g. calcite, gypsum) differ whether formed by surface or bulk crystallization (Karabelas et al., 2014, Xie and Gray, 2016), and may result in different degrees of scaling. Increased flux decline and decreased flux recovery has been observed during osmotic backwash for scaling via bulk versus surface crystallization (Cai et al., 2021). The presence of OM may reduce NF scaling by inhibiting mineral precipitation (Schäfer et al., 1998), or increase NF scaling by providing nucleation sites for surface crystallization (Wang et al., 2016). As scalants and OM may coexist in brackish and surface waters, fouling results from the simultaneous occurrence of Ca-enhanced OM fouling and scaling.

1.4. Role of inorganic scalants in nanofiltration fouling

Fouling mechanisms that occur when scalants and OM coexist are not fully understood, while it is certain that scalant-OM interactions contribute to both NF fouling and scaling (Tong et al., 2023). Wang et al. (2016) reported that OM types with high carboxylic group density, such as humic acid (HA) and sodium alginate (SA), provide nuclei for gypsum crystal growth accelerating surface crystallization as well as NF scaling. When considering bulk crystallization, inhibited growth of gypsum crystals was observed in the presence of HA, which was attributed to the blockage of growth sites on gypsum nuclei and distorted crystal morphology (Cao et al., 2022). Bovine serum albumin (BSA) and SA were revealed to inhibit gypsum crystal growth leading to reduced NF scaling, while contrasting results were reported for HA, which was thought to increase the bulk crystallization of gypsum as well as NF scaling (Lin et al., 2021). Characterization of fouling layers on membrane surfaces using advanced techniques has provided insight regarding fouling when scalants and OM coexist (Li et al., 2016; Ruiz-García et al., 2018; Tang et al., 2007a), while direct evidence in terms of specific Ca-OM interaction mechanisms is lacking. It is proposed that changes in the coordination environment of Ca and crystal structure of scalants following interactions with OM can be exploited to help elucidate fouling mechanisms when scalants and OM coexist. Such speciation and coordination environment information can be obtained at high resolution through synchrotron-based X-ray techniques.

1.5. Synchrotron-based X-ray techniques for fouling characterization

Synchrotron-based X-ray techniques provide a powerful tool to characterize complex fouling layers, helping to elucidate predominant NF fouling mechanisms. Common laboratory-based X-ray techniques,

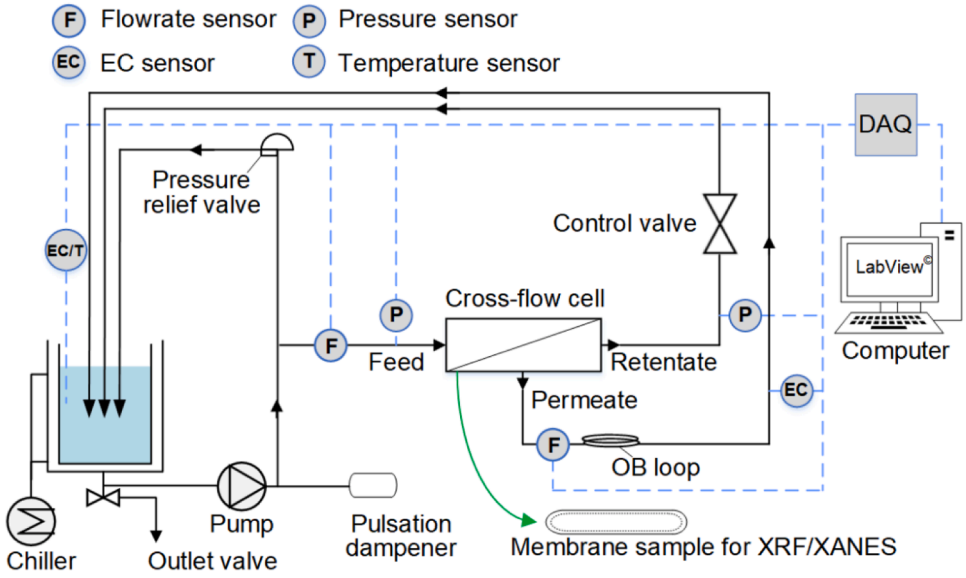

Fig. 2. Bench-scale crossflow filtration system.

such as energy dispersive X-ray spectroscopy (EDX), X-ray photoelectron spectroscopy (XPS), and X-ray diffraction (XRD), have been used to characterize fouling layers in terms of elemental composition as well as speciation, chemical environment, and crystalline structure, respectively (Park et al., 2024; Quay et al., 2018; Zheng et al., 2024). Limitations of common laboratory-based X-ray techniques include relatively low sensitivity to chemical speciation, high detection limits, shallow sample penetration depth, and long sample analysis times (Bone et al., 2020; Niemann et al., 2023). By comparison, synchrotron radiation light sources provide intense, tightly focused X-rays with a higher brightness over a wide range of energies (Adams 2010, Willmott 2019), which enables measurement of X-ray absorption spectroscopy (XAS) that provides information of the chemical species present in a sample. Synchrotron-based X-ray techniques have been applied for the characterization of membrane surface structure (Hou et al., 2023; Mitchell et al., 2011; Singh et al., 2012), solute-membrane interactions (Pignon et al., 2012), and foulant structure at the molecular level (Barry et al., 2020).

1.6. X-ray spectroscopy to characterize calcium-organic matter fouling

In XAS, elements (such as Ca within the fouling layers of membrane samples) are exposed to X-ray radiation, which can excite an inner shell electron to a higher energy state (Bone et al., 2020). Outer shell electrons then fill the hole left by the excited inner shell electron, emitting element-specific fluorescent radiation (Henderson et al., 2014). In X-ray fluorescence (XRF) imaging, the element-specific emission spectrum of a sample is recorded. Because the intensity of fluorescence at a certain energy is directly proportional to the mass of the element emitting at that energy, the element concentration can be obtained with this method (Bone et al., 2020). K-edge X-ray absorption near-edge structure (XANES) spectroscopy is sensitive to electronic transitions from the core 1s orbital of the innermost k-shell to antibonding molecular orbitals in outer shells, thus providing information on the electronic coordination environment of Ca present in membrane fouling layers (Rowley et al., 2023). Features associated with electronic transitions are observed at the rising edge and white line, which largely arise from 1s → p transitions (Henderson et al., 2014; Martin-Diaconescu et al., 2015). Thus, intensity and energy changes in the pre-edge feature and the white line imply changes to the electronic structure, hence the coordination environment of Ca. The post-edge region also varies as a result of coordination geometry, and is typically distinct for different minerals. Thus, it can be used in a finger-printing fashion to distinguish between Ca species, which exhibit distinct post-edge features based on their structures and crystallinity (Prietzel et al., 2021; Sowrey et al., 2004). When considering NF fouling, pre-edge features in XANES spectra of fouling layers may be indicative of unique bonds between Ca and membrane material (i.e. Ca conditioning) or Ca and OM (i.e. Ca-OM aggregation), while post-edge features associated with Ca structure and crystallinity could distinguish scaling mechanisms. Analyses of bulk samples are typically performed with a beam size of several hundred μm to several mm. In contrast, micro(μ)-XRF and μ−XANES enable imaging of ~mm^2-cm^2 sample areas using a small beam (1–100 μm) (Bone et al., 2020).

In the present study, synchrotron-based μ-XRF and μ-XANES are used to characterize NF membrane samples obtained following filtration experiments using feed solutions which contained: i) $CaCl_2$ only (as a baseline), ii) $CaCl_2$ with ten different OM types, and iii) $CaCO_3$ and $CaSO_4$ with humic acid (HA) to elucidate fouling mechanisms when scalants and OM coexist, as well as effects on flux decline and flux recovery during OB. Specific research questions are: i) Which Ca-enhanced OM fouling mechanism (Ca conditioning or Ca-OM aggregation) results in greater membrane flux decline? ii) Does the predominant Ca-enhanced OM fouling mechanism (Ca conditioning, Ca-OM aggregation) change as a function of OM type? iii) Can μ-XRF and μ-XANES be used to identify Ca-enhanced OM fouling and scaling mechanisms that occur when scalants and OM coexist?

2. Materials and methods

To determine which of Ca conditioning and Ca-OM aggregation fouling mechanisms contribute more to NF flux decline, two different types of filtration experiments were carried out; i) filtration of $CaCl_2$ feed solution followed by filtration of OM feed solution to provide Ca conditioning, and ii) filtration of a mixed $CaCl_2$-OM feed solution to induce Ca-OM aggregation. Then, the role of OM type in Ca-enhanced OM fouling was investigated using ten different OM types, grouped as humic substances, polyphenolic compounds, high molecular weight biopolymers, and low molecular weight compounds. To elucidate fouling and scaling mechanisms when scalants and OM coexist, filtration experiments were conducted using feed solutions with two typical scalants ($CaCO_3$, $CaSO_4$) and OM.

2.1. Bench-scale crossflow filtration system and membranes

Filtration experiments were performed using a bench-scale crossflow filtration system (Fig. 2), as previously described (Cai et al., 2021, Cai and Schäfer 2020). Briefly, the crossflow filtration system included a stainless steel crossflow cell (MMS Membrane Systems, Switzerland) with effective membrane area of 4.7×10^{-3} m^2. Filtration experiments were performed without a feed spacer to increase fouling/scaling rates and avoid interference with the CP layer. A stainless steel loop (2.1 m long, 1/8″ diameter, 166 mL volume) was incorporated into the permeate line directly following the crossflow cell to provide sufficient water volume for performing OB. Permeate and OB flowrates were monitored using a bi-directional liquid flow sensor (Sensirion SLS-1500, Switzerland). The crossflow filtration system was powered by a constant power output of 100 W (69 V). The opening of the control valve located downstream of the crossflow cell was fixed to maintain an operating pressure of 10 bar and crossflow velocity of approximately 0.4 m/s.

Commercial flat-sheet thin-film composite NF270 membranes (FilmTec™, DuPont Water Solutions, USA) were utilized in all filtration experiments as they are high flux, low retention membranes commonly used in brackish water desalination and surface water treatment applications. The active layer of NF270 membranes consists of semi-aromatic piperazine-based polyamide (Idil Mouhoumed et al., 2014) and has a molecular weight cut-off (MWCO) of 170 to 340 Da (Boussu et al., 2007; López-Muñoz et al., 2009). Reported $CaCl_2$ and NaCl retentions are 40% and 50%, respectively (López-Muñoz et al., 2009), and retention of humic acid (HA) >90% (Imbrogno et al., 2018).

2.2. Protocol for filtration experiments and membrane conditioning

Filtration experiments included: i) membrane pre-conditioning, ii) membrane compaction, iii) determination of membrane pure water permeability, iv) determination of the control valve set-point, v) filtration, vi) membrane sample preparation, and vii) bench-scale crossflow system cleaning. Pure water permeability of NF270 membranes used in this study ranged from 10–16 L/m^2h.bar, with 35–45% rejection of dissolved ions (measured as electrical conductivity) during filtration of feed solution containing 10 mM NaCl and 1 mM $NaHCO_3$ at an operating pressure of 10 bar. Detailed protocol for the filtration experiments is provided in Table S1.

2.3. Data analysis and error estimation for filtration experiments

Membrane performance during filtration experiments was characterized in terms of flux decline, flux recovery, and maximum OB flux, as described in previous work (Cai et al., 2022b). The mass of TOC deposited ($m_{deposit}$) on the membrane surface was determined by performing mass balance (Cai et al., 2022a). Additional details regarding membrane performance and error estimation analysis are provided in Section 2 of the SI.

Filtration experiments were performed using different feed solution chemistries to investigate the effect of Ca-enhanced OM fouling mechanisms, OM type, and the coexistence of scalants and OM on membrane performance. Filtration experiments were stopped following the third OB, and fouled membrane samples analyzed using X-ray spectroscopy to elucidate fouling mechanisms. Pure water flux measurements were not performed following filtration experiments to limit potential changes to the membrane fouling layer.

2.4. Feed solution chemistry and organic matter characteristics

The chemistry of feed solutions utilized during filtration experiments are shown in Table 1. For all filtration experiments, feed solutions contained $CaCl_2{\cdot}H_2O$ (VWR Chemicals, ≥99.8%, Germany). When considering Ca-OM bridging and complexation, as well as OM type (experiments 2–13), 10 mM NaCl (Merck Millipore, ≥99.5%, Germany) and 1 mM $NaHCO_3$ (Merck Millipore, ≥99.7%, Germany) provided background electrolytes. For the coexistence of scalants and OM, $CaCO_3$ and $CaSO_4$ were selected as model scalants due to their prevalence in natural waters (Chong and Sheikholeslami, 2001, Dydo et al., 2003; Tong et al., 2023) and limited solubility, which makes them important contributors to scaling in high pressure membrane systems (Antony et al., 2011). Scalants were produced in-situ using inorganic salts: $CaCl_2{\cdot}H_2O$ and $NaHCO_3$ for $CaCO_3$, and $CaCl_2{\cdot}H_2O$ and Na_2SO_4 (Honeywell Fluka, ≥99.0%, Germany) for $CaSO_4$. The final feed solution concentrations of $CaCO_3$ and $CaSO_4$ were equivalent to those previously observed to induce surface crystallization at saturation indexes of 1.25 and 1.63, respectively (Cai et al., 2021). Based on Ca concentrations reported for groundwater (2.9–841.4 mg/L) (Al Haj et al., 2023) as well as seawater (400 mg/L) (Mewes et al., 2014), and that Ca complexes with CO_3 and SO_4 to form $CaCO_3$ and $CaSO_4$, the selected concentration

Table 1
Chemistry of feed solutions used during filtration experiments.

Experiment number	Parameter	Background solution	Mineral types	Mineral concentration (mM)	Organic matter type	TOC (mgC/L)
1	Baseline	MilliQ + 1 mM $NaHCO_3$ + 10 mM NaCl	$CaCl_2$	1.5	None	0
2	Ca conditioning		$CaCl_2$	1.5	HA	5
3			$CaCl_2$	1.5	TA	5
4	Ca-OM aggregation		$CaCl_2$	1.5	HA	5
5			$CaCl_2$	1.5	TA	5
6	OM type		$CaCl_2$	1.5	GLU	5
7			$CaCl_2$	1.5	FP	5
8			$CaCl_2$	1.5	AUS	5
9			$CaCl_2$	1.5	WF	5
10			$CaCl_2$	1.5	BSA	5
11			$CaCl_2$	1.5	TANN	5
12			$CaCl_2$	1.5	TEA	5
13			$CaCl_2$	1.5	SA	5
14	Scaling	MilliQ	$CaCl_2$	4	None	0
			$NaHCO_3$	8		
15			$CaCl_2$	25	None	0
			Na_2SO_4	61		
16	Combined Ca-OM fouling		$CaCl_2$	4	HA	5
			$NaHCO_3$	8		
17			$CaCl_2$	25	HA	5
			Na_2SO_4	61		
18			$CaCl_2$	29	HA	5
			$NaHCO_3$	8		
			Na_2SO_4	61		

of $CaCO_3$ is within the range of natural waters, while that of $CaSO_4$ is higher. Similar concentrations of scalants have been applied in previous studies to accelerate membrane scaling (Mi and Elimelech, 2010; Wang et al., 2016). Feed solutions containing $CaCO_3$ alone and $CaCO_3$ with 5 mgC/L OM contained an additional 61 mM NaCl in order to maintain similar osmotic pressure to $CaSO_4$ feed solutions. For all feed solutions, pH was adjusted to 8.0±0.1 using 1 M NaOH (Merck Millipore, ≥99%, Germany) or 1 M HCl (diluted from 37% HCl, VWR Chemicals, Germany).

Ten OM types were grouped as: i) humic substances - humic acid (HA), Australian natural organic matter (AUS), and worm farm extract (WF), ii) polyphenolic compounds - tannic acid (TA), Indian tea (TEA), and tannin (TANN), iii) high molecular weight biopolymers - sodium alginate (SA) and bovine serum albumin (BSA), and iv) low molecular weight compounds - fermented product (FP) and glucose (GLU). OM characteristics, as previously reported (Cai et al., 2022b; Nguyen et al., 2021), are provided in Table 2. HA and TA were selected for Ca conditioning and Ca-OM aggregation experiments (experiment numbers 2–5), as these OM types are known to complex strongly with Ca (Cai et al., 2022b). HA was utilized during filtration experiments designed to investigate fouling when scalants and OM coexist due to its prevalence in groundwater (Lipczynska-Kochany 2018) as well as seawater (Adusei-Gyamfi et al., 2019), and its previously observed effects on bulk (Cao et al., 2022; Curcio et al., 2010) and surface (Benecke et al., 2018) crystallization.

2.5. Analytical methods for water quality

For samples collected during filtration experiments performed using different OM types, total organic carbon (TOC) concentrations were determined using a TOC analyzer (Sievers M9, SUEZ, France). A sample instrument calibration curve for the TOC analyzer is provided in the SI (Figure S1). For all filtration experiments, temperature and pH of feed solutions (Figure S2) as well as electrical conductivity (EC) of feed solutions and permeate were measured using a pH/EC meter (pH/Cond 3320, WTW, Germany) (Figure S3 to Figure S6).

2.6. Membrane preparation and characterization

To prepare membrane samples following filtration experiments, fouled membranes were gently removed from the crossflow filtration cell, and rinsed with MilliQ water to remove any feed solution that may have remained on the membrane surface. Membrane samples were left to dry overnight under atmospheric conditions at room temperature (21 ±1 °C). Sample photos of prepared membrane samples from filtration experiments (experiment numbers 16–18) are presented in Figure S7.

Five membrane samples obtained following filtration experiments designed to investigate fouling when scalants and OM coexist were analyzed using field-emission scanning electron microscopy (FE-SEM, Gemini, Carl Zeiss Research Microscopy Solutions, Germany) at IOM Leipzig, Germany. To obtain a cross-section, membrane samples were prepared according to a previously described method (Cai et al., 2021). Briefly, membrane samples were dipped into tissue freezing liquid (Leica, Ref-14020108926, UK) then placed inside a cryo-microtome (Leica, CM 1860UV, Germany) and cut at -30ºC using a stainless steel knife. Membrane samples were then soaked in MilliQ water to remove the tissue freezing liquid, and dried again under atmospheric conditions. Prior to imaging with FE-SEM, dried membrane samples were coated with a 5 nm platinum layer using a high resolution sputter coater (Cressington Scientific Instruments, 208 HR, UK) at an acceleration voltage of 3 keV (EHT) and coating time of approximately 25 s. Secondary electrons were detected with the chamber Everhart Thornley detector. FE-SEM analysis included imaging at 3–5 random locations using 300–75,000 times magnification. Images were obtained at 2048 pixels using a field of view (i.e. approximate size of observable objects) ranging from several μm up to 1000 μm.

Dried membrane samples from filtration experiments using $CaCl_2$ (baseline), $CaCl_2$ and ten different OM types, as well as $CaCO_3$ + $CaSO_4$ + HA were sent for synchrotron-based XRF and XANES spectroscopy *ex-situ* analyses at the Stanford Synchrotron Radiation Lightsource (SSRL).

2.7. Spatial distribution of calcium: X-ray fluorescence (XRF)

To visualize the spatial distribution as well as quantify the mass of Ca deposition in the membrane fouling layer, membrane samples were analyzed using XRF (Fig. 3).

Two-dimensional maps of membrane samples were obtained using μ-XRF at SSRL beamlines 14–3 and 7–2, both using Si(111) double crystal monochromators to select the incident energy. Beamline 14–3 has high spatial resolution (5 μm), but a relatively small field of view (~mm^2), whereas beamline 7–2 has low spatial resolution (100 μm) but a large field of view (~cm^2). When possible, samples were imaged at beamline 7–2, which allowed us to map the Ca distribution across the entire membrane surface. At beamline 14–3, we mapped smaller regions at higher spatial resolution. Beamline 14–3 is a tender X-ray beamline, with an energy range between 2100 and 5000 eV, enabling us to measure Ca K-edge μ-XANES spectra in addition to mapping Ca fluorescence. Beamline 7–2 is a hard X-ray beamline (5000–16,200 eV), and so cannot access the Ca K-edge. Samples were measured at room temperature, either open to the air (beamline 7–2), or in a He atmosphere (beamline 14–3).

At beamline 7–2, images of membranes were collected at a scanning step size of 100 μm and an incident energy of 7000 eV. At beamline 14–3, images of the membranes were collected as the samples were scanned across the X-ray beam at a step size of 5 μm and an incident energy of 4150 eV. At both beamlines 7–2 and 14–3, Ca K-alpha fluorescence was detected using a seven element Vortex Si-drift detector. The concentration of Ca (μg/cm^2) on membrane samples was determined by image analysis using Sam's Microanalysis Toolkit (SMAK) (Webb 2011) and a reference Ca foil of known concentration: CaF_2 (56.8 μg/cm^2).

In addition to single energy maps, multi-energy (ME) maps were

Table 2
Molecular characteristics of different organic matter types (Cai et al., 2022b; Nguyen et al., 2021).

Organic compound	Molecular weight (Da)	$SUVA_{254}$ (L/mgC.m) aromaticity	Carboxyl group density (mmol/gC)	Phenolic group density (mmol/gC)	Charge density (μeq/mgC.L)	Preferable functional groups for Ca^{2+}-bridging
HA	780	10 ± 0.7	7.5 ± 0.5	6.7 ± 0.6	9.5 ± 0.3	Carboxylic, phenolic groups
AUS	530	3.1 ± 0.3	5.2 ± 0.5	4.3 ± 0.5	1.7 ± 0.1	
WF	–	5.4 ± 0.5	1.7 ± 0.4	3.1 ± 0.5	7.7 ± 0.4	–
TA	1701	14 ± 0.5	4.8 ± 0.6	13.5 ± 1.5	3.6 ± 0.1	Phenolic hydroxyl groups
TEA	380	2.8 ± 0.3	0.7 ± 0.3	3.2 ± 0.6	4.0 ± 0.1	–
TANN	23,000	5.2 ± 0.5	0.1 ± 0.06	2.6 ± 0.6	4.2 ± 0.1	–
SA	>120,000	0.1 ± 0.01	10 ± 1	8 ± 0.8	14.6 ± 0.1	Hydroxyl groups (Helmiyati and Aprilliza 2017)
BSA	66,500	0.12 ± 0.01	9.3 ± 0.9	6.7 ± 0.6	1.9 ± 0.2	Amino, carboxyl groups
FP	480	0.1 ± 0.01	2.4 ± 0.3	1.0 ± 0.4	0.1 ± 0.2	–
GLU	180	0.1 ± 0.01	0.01 ± 0.01	0.02 ± 0.01	0.1 ± 0.2	Hydroxyl group (weak binding)

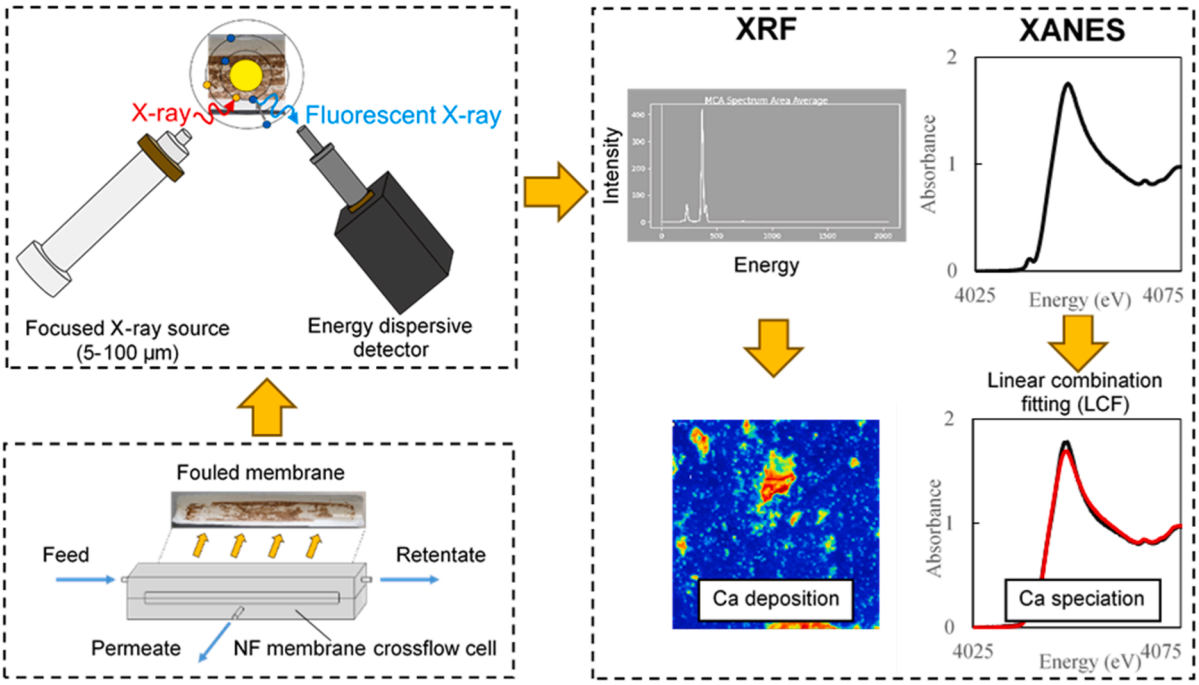

Fig. 3. X-ray fluorescence (XRF) and X-ray absorption near edge structure (XANES) spectroscopy analyses of a nanofiltration membrane samples obtained following filtration experiments.

collected across the Ca K-edge (4045.48, 4049.36, 4051.46, and 4059.53 eV) for select samples to ascertain whether different Ca species were distributed across the membrane. These energies were chosen because they correspond to specific features (i.e. large peaks) in the Ca K-edge XANES spectrum of gypsum and calcite. Principal component analysis (PCA) was performed on ME maps and Ca K-edge µ-XANES spectra collected at membrane sample locations which exhibited the greatest difference in eigenvalues (as determined using SMAK). As eigenvalues represent the variance of each principal component from Ca K-edge µ-XANES spectra, the selected membrane sample locations corresponded to those which demonstrated the greatest difference in Ca coordination environment. "XANES fitting" of the ME maps was performed in SMAK; in this procedure, each pixel is fit as a linear combination of reference materials based on the intensity at each energy (i.e. 4045.48, 4049.36, 4051.46, and 4059.53 eV). This procedure is described in detail in a previous study (Farfan et al., 2018). The reference materials used included Ca-HA, $CaSO_4$, and calcite, since these were the materials that we expected to find based on the feed solution chemistry. In this way, we were able to examine the distribution of calcium species- organic and mineral- across the membrane surface. Ca K-edge µ-XANES spectra were fit as linear combinations of reference XANES spectra (see description of this method below), using the following reference materials: Ca-HA, Ca adsorbed to the membrane, calcite, vaterite, aragonite, amorphous calcium carbonate (ACC), gypsum, as well as the membrane sample spectrum from the filtration experiment using $CaSO_4$ alone, which may have included anhydrite and bassanite polymorphs. These references were chosen based on performing PCA on the µ-XANES, followed by target transform analysis (TTA): if a reference spectrum can be reconstructed using the significant components identified by PCA this indicates that the reference material is representative of a species that is found within the sample (Calvin, 2013; Niemann et al., 2023). In contrast, if a reference material cannot be reconstructed from the sample spectra principal components, then it is absent from the mixture of species that comprise the sample.

2.8. Speciation of calcium: X-ray absorption near-edge structure (XANES) spectroscopy

X-ray absorption near-edge structure (XANES) spectroscopy was used to identify Ca species (Calvin, 2013; Henderson et al., 2014) (Ca-OM aggregates, calcite/gypsum crystals) deposited on or bound to membrane samples. Ca K-edge XANES has been previously utilized to assess Ca speciation in membrane systems (Kum et al., 2021; Niemann et al., 2023). Monochromator calibration was performed by setting the first derivative of a $CaSO_4$ spectrum to 4043.89 eV. For membrane samples from filtration experiments which considered different OM types, bulk Ca K-edge XANES spectra were collected using a 1×1 mm beam.

Linear combination fitting (LCF) of XANES spectra from membrane samples was performed to determine the relative amounts of Ca bound to the membrane (Ca conditioning) versus Ca-OM aggregation. LCF involves the least-squares fitting of XANES spectra from membrane samples with a linear combination of reference spectra (Calvin 2013, Ravel and Newville 2005). XANES spectra for baseline ($CaCl_2$ only) and Ca-HA filtration experiments were used as LCF references (Figure S9). The baseline spectrum corresponds to Ca bound to the membrane (Ca conditioning). The Ca-HA sample exhibited the highest concentration of Ca on the membrane when compared to other OM types, which was considered representative of a Ca coordination environment unique to Ca-OM aggregation (Cai et al., 2022b) with negligible signal from the baseline. Ca bound to the membrane could bridge OM moieties in the bulk solution with ligands on the membrane surface (Iskrenova-Tchoukova et al., 2010) and provide charge screening to increase membrane surface charge and OM deposition (Shim et al., 2002). Prior to deposition onto the membrane, Ca-OM aggregation in the bulk solution could have been by cationic bridging or the formation of bonds between Ca and OM molecules (Adusei-Gyamfi et al., 2019).

Ca K-edge µ-XANES spectra were normalized by fitting a third-order polynomial function from 4063.8 eV to 4131.5 eV and background subtracted by fitting a linear function from 4013.8 eV to 4033.8 eV using Athena software (Ravel and Newville 2005). Spectra for samples containing Ca and nine (10 minus HA, which served as a reference) different

OM types were fit as a linear combination of the reference spectra to assess the extent to which the Ca coordination environment differed from the baseline, and whether the Ca complexed by different OM types exhibited similar or distinct coordination environments. Spectra were fit between 4023.8 to 4072.8 eV. LCF was performed in Athena, from which fraction values were obtained representing the amount of Ca bound to the membrane and bound to OM. Higher Ca-HA fraction values indicated Ca-OM aggregation, while higher baseline fraction values indicated Ca was bound to the membrane (Ca conditioning). The goodness of fit was quantified in Athena by the R-factor, which represents the percent of misfit between measured data and LCF results (Calvin 2013). Further details regarding R-factor calculations for LCF are provided in the SI.

3. Results and discussion

Ca-OM interactions contribute to both NF fouling and scaling (Tong et al., 2023), however Ca-enhanced OM fouling and scaling mechanisms that occur when scalants and OM coexist are not fully understood. To elucidate the role of Ca, OM type, as well as the coexistence of scalants ($CaCO_3$, $CaSO_4$) and OM in NF fouling, synchrotron-based XRF and XANES were used to characterize Ca within the fouling layer of NF membrane samples obtained following filtration experiments.

3.1. Contribution of conditioning and aggregation mechanisms to NF fouling

Ca conditioning and Ca-OM aggregation have been identified as the main Ca-enhanced OM fouling mechanisms (Lee et al., 2021; Yoon et al., 1998), however their relative contribution to membrane flux decline remains unclear. To determine which Ca-enhanced OM fouling mechanism results in greater membrane flux decline, filtration experiments were conducted that were designed to induce Ca conditioning and Ca-OM aggregation (Fig. 4). HA and TA were utilized in feed solutions as these OM types were previously observed to increase flux decline and reduce flux recovery during OB when compared to other OM types (Cai et al., 2022b). Mass balance results for TOC deposition are provided in Figure S8.

When considering both HA and TA, greater flux decline was observed for Ca-OM aggregation when compared to Ca conditioning. While increased flux decline observed for the NF treatment of feed solutions containing Ca and OM (HA, SA) has been attributed to Ca-OM aggregation (Lee et al., 2021), Ca conditioning and Ca-OM aggregation mechanisms were not distinguished. In the present study, the magnitude of flux decline observed for Ca conditioning were similar for HA and TA (20%), despite differences in OM characteristics (Table 2). For Ca-OM aggregation, flux decline was dictated by Ca-OM interactions in the bulk solution and subsequent deposition of Ca-OM aggregates on the membrane surface. The higher overall functional group (carboxyl, phenolic) density as well as larger size (1701 vs. 780 Da) of TA vs. HA molecules could result in the deposition of comparatively large Ca-OM aggregates which increase CP and cake formation. Trends observed during filtration experiments indicate that Ca-OM aggregation and deposition is the main driver of flux decline when compared to Ca conditioning.

While greater flux decline was observed for Ca-OM aggregation versus Ca conditioning, additional evidence is required to validate the occurrence of these Ca-enhanced OM fouling mechanisms.

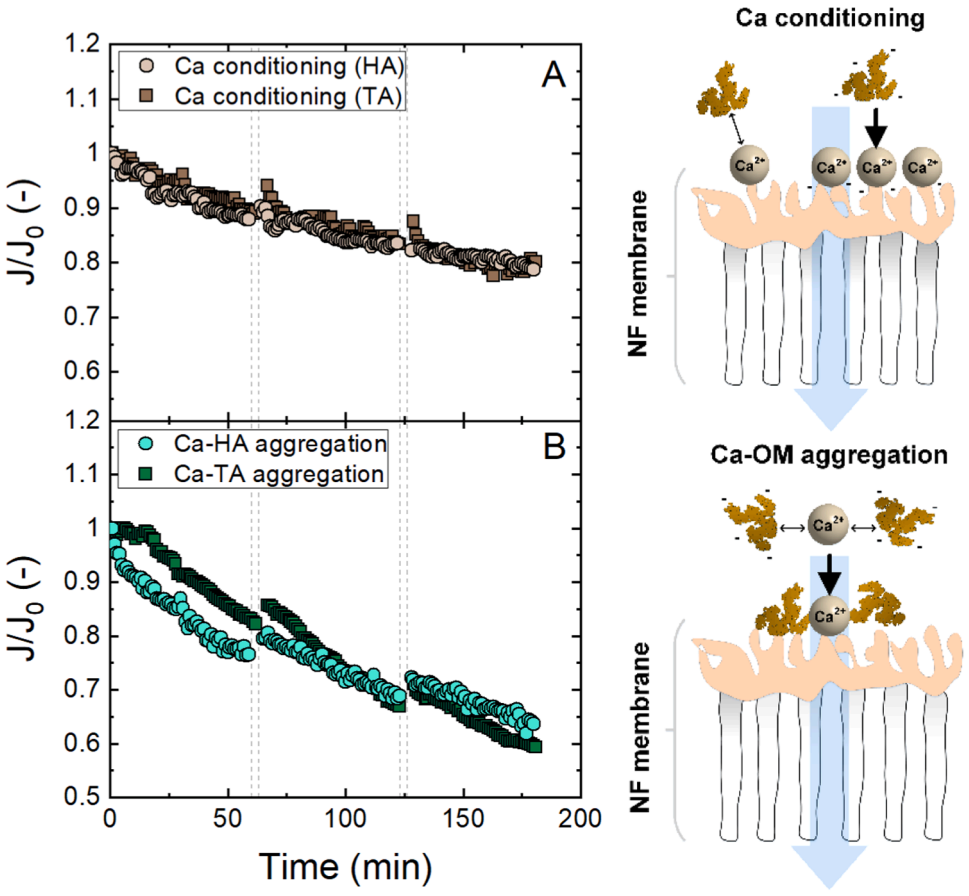

Fig. 4. Normalized flux for (A) Ca conditioning (1.5 mM $CaCl_2$ followed by 5 mgC/L OM) and (B) Ca-OM aggregation (1.5 mM $CaCl_2$ mixed with 5 mgC/L OM). (pH 8.0±0.1, 24±1 °C).

3.2. Quantification of calcium deposition for conditioning and aggregation mechanisms

To obtain evidence for the occurrence of Ca conditioning and Ca-OM aggregation mechanisms, Ca deposition on membrane samples was quantified using μ-XRF (Fig. 5). Based on greater flux decline and lower flux recovery during OB, increased Ca deposition was anticipated for Ca-OM aggregation versus Ca conditioning experiments.

Greater deposition of Ca was observed on membrane samples for Ca-OM aggregation versus Ca conditioning experiments, which supports the occurrence of Ca-OM aggregation. Similarly, greater deposition of Ca and flux decline was reported during the NF treatment of feed solution containing Ca and HA versus Ca alone, which was attributed to Ca-HA aggregation (Lee et al., 2021). In the present study, despite higher maximum OB flux (i.e. flow rate per membrane surface area from the permeate side to the feed side of the membrane) for Ca-OM aggregation, flux recovery was lower when compared to Ca conditioning. Higher maximum OB flux for Ca-OM aggregation is attributed to greater Ca deposition, which enhanced CP (Benecke et al., 2018) but provided insufficient driving force to displace the fouling layer and attain similar levels of flux recovery as those observed for Ca conditioning (Cai et al., 2022b).

Membrane flux decline and recovery following OB have been observed to vary as a function of OM type (Cai et al., 2022b; Lee et al., 2021). In the next section, to reveal how the predominant Ca-enhanced OM fouling mechanism changes as a function of OM type, filtration experiments were performed with different OM types and then membrane samples were analyzed using μ-XRF and XANES.

3.3. Contribution of organic matter type to NF fouling mechanisms

To investigate the role of OM type in Ca-enhanced OM fouling and membrane flux, filtration experiments were conducted using ten different types of OM grouped into four general categories: humic substances, polyphenolic compounds, high molecular weight compounds, and low molecular weight compounds. Membrane flux was quantified in terms of normalized flux, flux decline, and flux recovery following OB (Fig. 6). It was anticipated that OM types which most readily formed complexes with Ca would result in the greatest membrane flux decline.

Substantial flux decline (13~36%) and low flux recovery (8~31%) were observed for TEA, HA, TA, and SA. HA, TA, and SA exhibit relatively high carboxyl group and negative charge densities (Table 2) (Cai et al., 2022b), which can facilitate complexation with Ca and charge neutralization (Adusei-Gyamfi et al., 2019, Lee and Elimelech 2006) inhibiting charge repulsion between OM and the negatively charged membrane surface. As such, through interactions with Ca, OM types which have both comparatively high carboxyl group density as well as negative charge density may contribute more to membrane flux decline than other OM types. While TEA has relatively low carboxyl group density, it is abundant in tannins (Khasnabis et al., 2015) that can complex with Ca and enhance sorption to the membrane (Li et al., 2019).

Having identified OM types which resulted in high and low flux decline, additional evidence was required to verify which of Ca conditioning or Ca-OM aggregation was the predominant fouling mechanism.

3.4. Quantification of calcium deposition on NF membranes

To obtain visual evidence of Ca conditioning and Ca-OM aggregation mechanisms, mapping of Ca deposition within the fouling layer of membrane samples was performed using μ-XRF (Fig. 7). Greater Ca deposition due to Ca-OM aggregation was anticipated for high flux decline OM types (TEA, HA, TA, SA) when compared to other OM types.

Ca deposition was greatest for the high flux decline OM types (TEA,

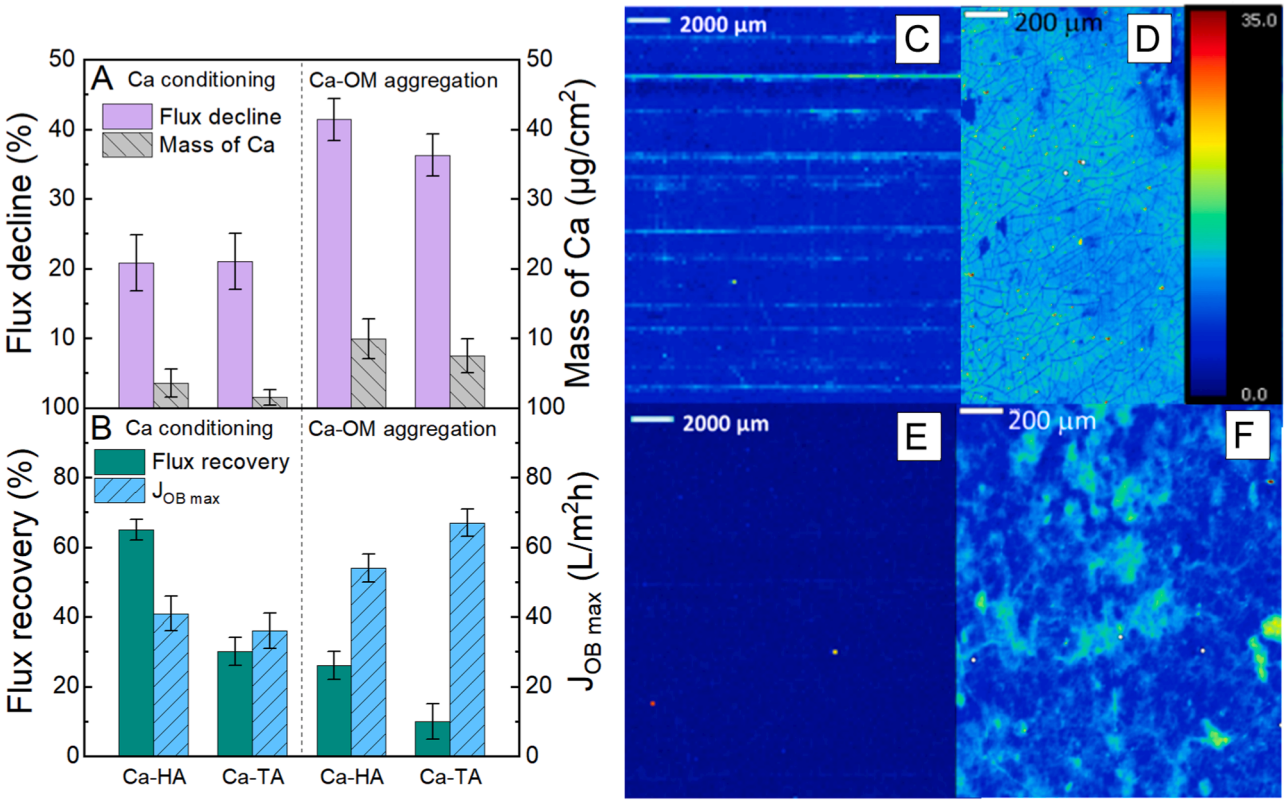

Fig. 5. (A) flux decline and average mass of Ca deposited per membrane surface area, and (B) flux recovery during OB and maximum OB flux for Ca conditioning and Ca-OM aggregation. Ca-HA data was adapted from previous work (Cai et al., 2022a). Surface mapping of Ca deposition (0–35 μg/cm^2) on membrane samples for (C) Ca conditioning (HA), (D) Ca-HA aggregation, (E) Ca conditioning (TA), and (F) Ca-TA aggregation. (pH 8.0±0.1, 24±1 °C).

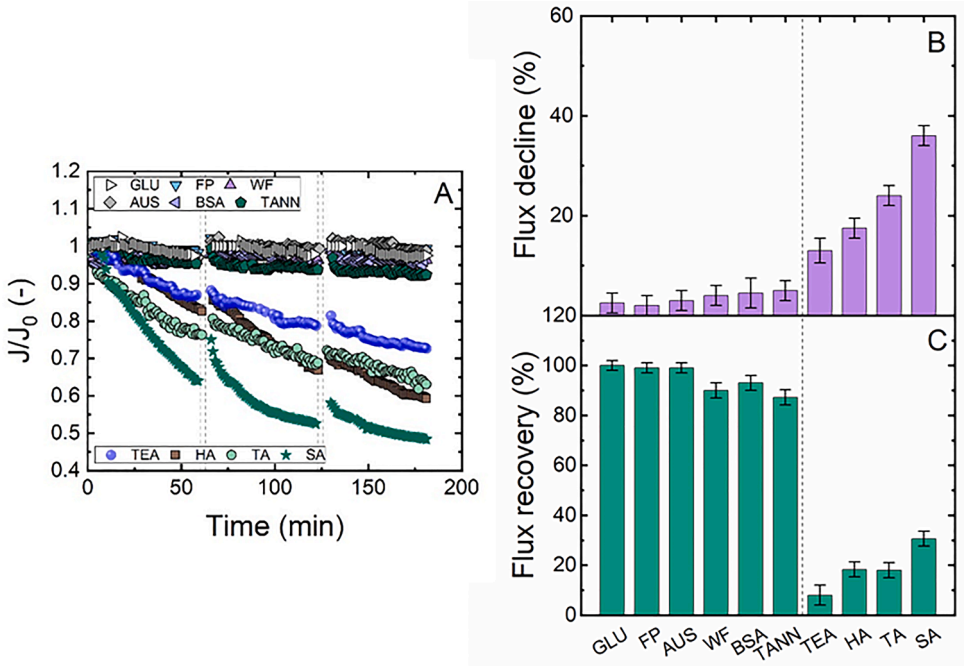

Fig. 6. (A) normalized flux, (B) flux decline, and (C) flux recovery following OB for Ca mixed with different OM types. (5 mgC/L OM, 1.5 mM $CaCl_2$, 10 mM NaCl, 1 mM $NaHCO_3$, pH 8.0±0.1, 24±1 °C).

HA, TA, SA), suggesting the occurrence of Ca-OM aggregation, while Ca deposition for the remaining OM types was comparable to the baseline. Surface maps reveal continuous layers of Ca deposited on membranes for HA, SA, and TA, while TA is unique in that the surface map exhibits numerous hot spots on top of the background Ca.

To quantify Ca deposition on membrane samples, μ-XRF data was analyzed using Sam's Microanalysis Toolkit (SMAK) software (Fig. 8). Ca deposition on the membrane sample from filtration of $CaCl_2$ only (without OM) served as a baseline (BL). To quantify the deposition of OM, mass balance was performed using TOC concentrations in the membrane feed, retentate, and permeate.

The average mass of Ca deposited on membrane samples for high flux decline OM types (HA, TA, TEA, SA) was greater when compared to other OM types, and corresponded with high TOC deposition as well as flux decline and low flux recovery observed during filtration experiments. High Ca deposition and flux decline was reported during NF treatment of feed solution containing HA and $CaSO_4$, which also corresponded with increased flux decline (Lin et al., 2021). In contrast to this study, the authors observed low Ca deposition and flux decline when considering SA, potentially due to differences in the type of SA that was utilized. The average mass of Ca deposited on membrane samples for other OM types (GLU, FP, AUS, WF, BSA, TANN) was similar to the baseline, suggesting limited complexation with Ca. Low TOC deposition (GLU, FP, AUS, WF) provides further evidence of limited complexation with Ca, while greater deposition of BSA and TANN was due to high molecular weights. Differences in the concentration of Ca and TOC deposited on the membrane between OM types indicates that OM type affects Ca-enhanced OM fouling mechanisms.

To determine if flux decline and Ca deposition observed for different OM types corresponded with Ca speciation characteristic of Ca conditioning or Ca-OM aggregation, the fouling layer of membrane samples was analyzed using XANES.

3.5. Calcium speciation for different organic matter types

XANES spectra were obtained for membrane samples from filtration experiments with different OM types, and linear combination fitting (LCF) (Section 2.8) performed using the baseline (BL) and Ca-HA sample spectra as references (Fig. 9). Features in the pre-edge and edge regions (located to the left of the peak), as well as the white line (peak), are dependent on the Ca coordination environment, while post-edge features (located to the right of the peak) are dependent on long range structure and crystallinity. Fraction values from LCF, representing the proportion of BL and Ca-HA reference spectra (Figure S9) that can be fitted to XANES spectra, are provided in Table 3. XANES spectra that were fitted with a greater fraction of the Ca-HA spectrum indicated that Ca-OM aggregation was predominant, while spectra that were fitted with a greater fraction of the baseline spectrum indicated Ca bound to the membrane, which can interact with OM in the bulk solution and provide charge screening of the membrane surface.

Ca-HA represented a large fraction of the XANES spectra for high flux decline OM types (TEA, TA, SA) and the concentration of Ca on the membrane for these high flux decline OM types was greater than that of the baseline (Fig. 8). This suggests that the majority of Ca in the fouling layer was complexed by OM and exhibited a coordination environment similar to that observed for Ca-HA. For low flux decline OM types, the baseline represented a greater fraction of the sample spectra for AUS, BSA, and TANN, suggesting that Ca was predominantly bound to the membrane. That WF and FP could not be fitted using LCF, suggests another Ca-OM end member is needed to represent the Ca coordination environment of these samples. Based on their XANES spectra, the majority of Ca in WF and FP samples may be bound to the membrane with some of the remaining fraction bound to OM in a coordination environment that is distinct from HA. For GLU, Ca-HA represented a large fraction of the XANES spectrum, implying that although the mass of Ca deposited on the membrane was lowest among all OM types, that which was deposited formed complexes with OM.

OM contains numerous functional groups that provide sites for binding with Ca. In this study, XANES spectra represent an average of all of the Ca coordination environments present within the fouling layer of a membrane sample, which were fitted using reference spectra to determine if Ca was predominantly bound to the membrane or aggregated with OM. This approach is limited in that factors other than the local coordination environment of Ca may contribute to Ca-enhanced OM fouling. For example, XANES cannot probe the structure of Ca-OM aggregates, the extent to which Ca bound to the membrane interacts

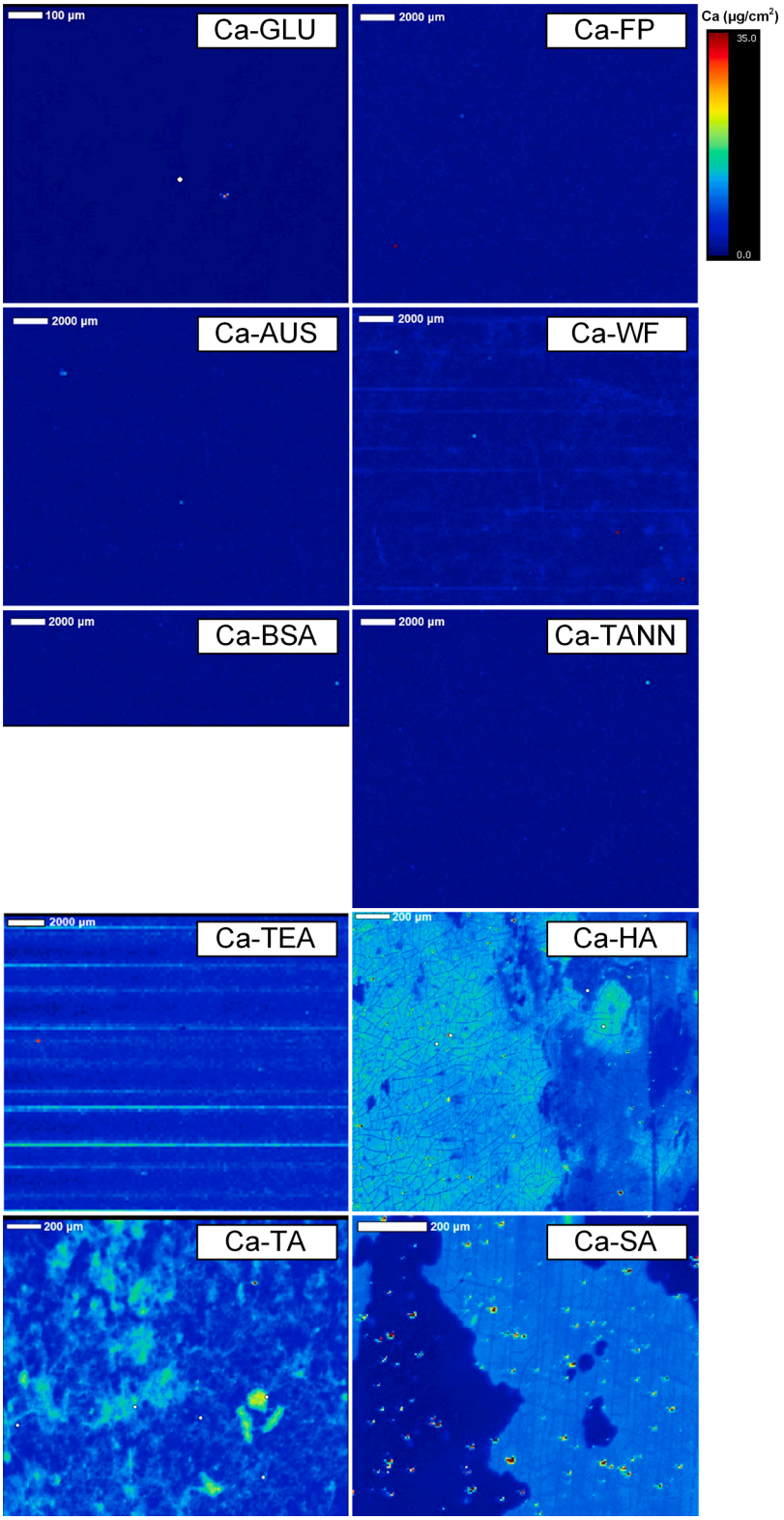

Fig. 7. Surface mapping of Ca deposition (0–35 µg/cm^2) within the fouling layer on membrane samples for Ca mixed with different OM types. (5 mgC/L OM, 1.5 mM $CaCl_2$, 10 mM NaCl, 1 mM $NaHCO_3$, pH 8.0±0.1, 24±1 °C).

with OM in the bulk solution, or whether chemically labile Ca that was bound to the membrane diffuses back into the bulk and contributes to OM aggregation. To account for these limitations and obtain a comprehensive understanding of flux decline trends observed during filtration experiments, it was important to quantify Ca and TOC deposition.

In natural waters Ca containing scalants, such as calcium carbonate ($CaCO_3$) and calcium sulphate ($CaSO_4$), coexist with OM. As such, it is necessary to understand which Ca-enhanced OM fouling and scaling mechanisms predominate when scalants and OM coexist, as well as how $CaCO_3$ and $CaSO_4$ crystallization may change in the presence of OM.

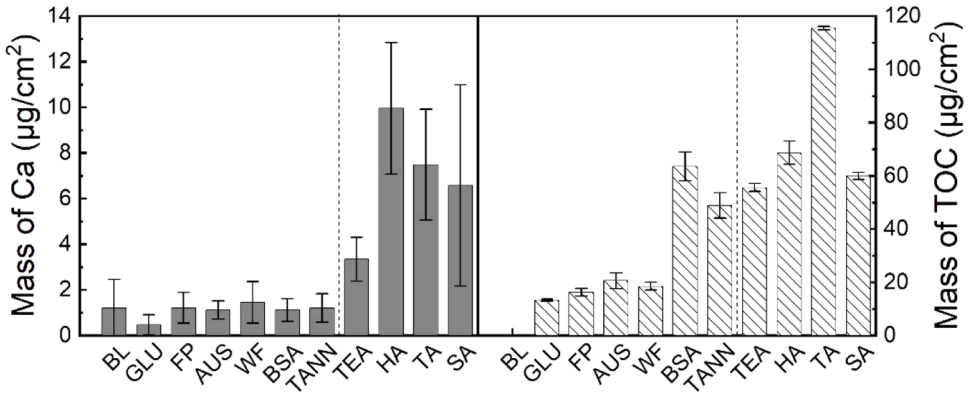

Fig. 8. Average mass of Ca and TOC deposited within the fouling layer per membrane surface area for membrane samples for Ca mixed with different OM types. BL = baseline ($CaCl_2$). (5 mgC/L OM, 1.5 mM $CaCl_2$, 10 mM NaCl, 1 mM $NaHCO_3$, pH 8.0±0.1, 24±1 °C). Error bars for the mass of Ca represent its variation across the entire area of the membrane that was analyzed; error bars for the mass of TOC represent the absolute error (max/min) from repeated measurements.

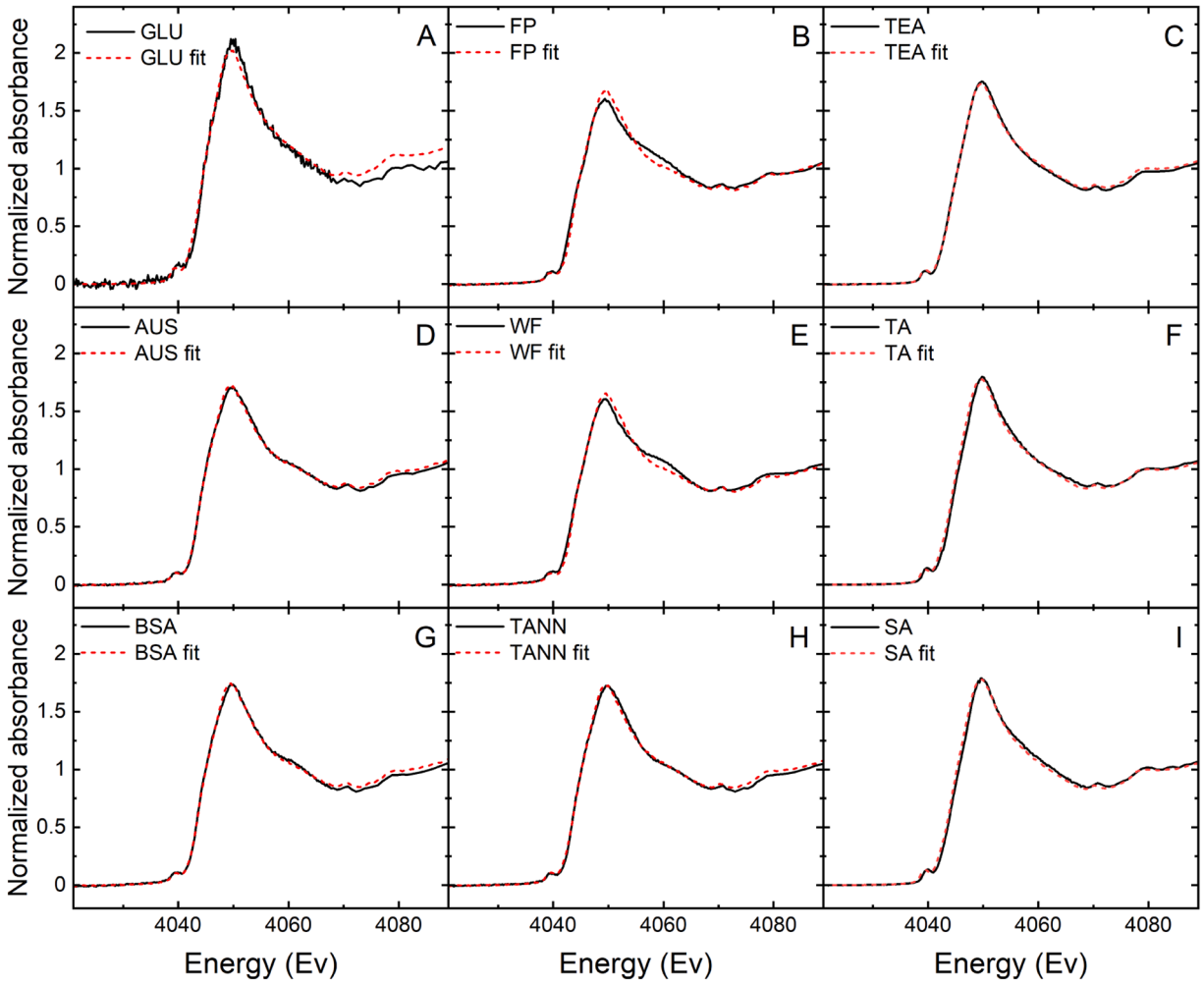

Fig. 9. Normalized Ca K-edge XANES spectra for the fouling layer on membrane samples for Ca mixed with different OM types. (5 mgC/L of OM, 1.5 mM $CaCl_2$, 1 mM $NaHCO_3$, 10 mM NaCl, pH 8.0±0.1, 24±1 °C).

3.6. NF fouling mechanisms when scalants and organic matter coexist

To investigate the effect of Ca-enhanced OM fouling (Ca conditioning, Ca-OM aggregation) and scaling mechanisms on membrane flux when scalants and OM coexist, filtration experiments were conducted using feed solutions with: i) 4 mM $CaCO_3$ alone ($CaCO_3$ scaling), ii) 4 mM $CaCO_3$ with 5 mgC/L HA ($CaCO_3$ + HA), iii) 25 mM $CaSO_4$ alone ($CaSO_4$ scaling), iv) 25 mM $CaSO_4$ with 5 mgC/L HA ($CaSO_4$ + HA), and v) 4 mM $CaCO_3$ and 25 mM $CaSO_4$ with 5 mgC/L HA ($CaCO_3$ + $CaSO_4$ + HA). Membrane flux was quantified in terms of normalized flux, flux decline, and flux recovery following OB (Fig. 10).

Filtration experiments using HA with $CaCO_3$ exhibited greater flux decline and lower flux recovery than $CaCO_3$ alone as well as Ca-HA, while HA with $CaSO_4$ had similar flux decline and recovery when

Table 3
Fraction values from linear combination fitting (LCF) of XANES spectra for the fouling layer of membrane samples using baseline and Ca-HA spectra as references.

OM type	Fraction of Ca-HA	R-factor	Fraction of baseline	R-factor	Sum of fractions
Low flux decline OM types					
Ca-GLU	0.89	0.09	0.18	0.08	1.07
Ca-FP	0.00	0.09	1.00	0.10	1.00
Ca-AUS	0.13	0.04	0.89	0.04	1.02
Ca-WF	0.03	0.08	0.96	0.08	0.98
Ca-BSA	0.16	0.04	0.88	0.04	1.03
Ca-TANN	0.38	0.04	0.65	0.04	1.02
High flux decline OM types					
Ca-TEA	0.94	0.03	0.07	0.03	1.00
Ca-TA	0.95	0.07	0.00	0.06	0.95
Ca-SA	0.96	0.06	0.00	0.00	0.96

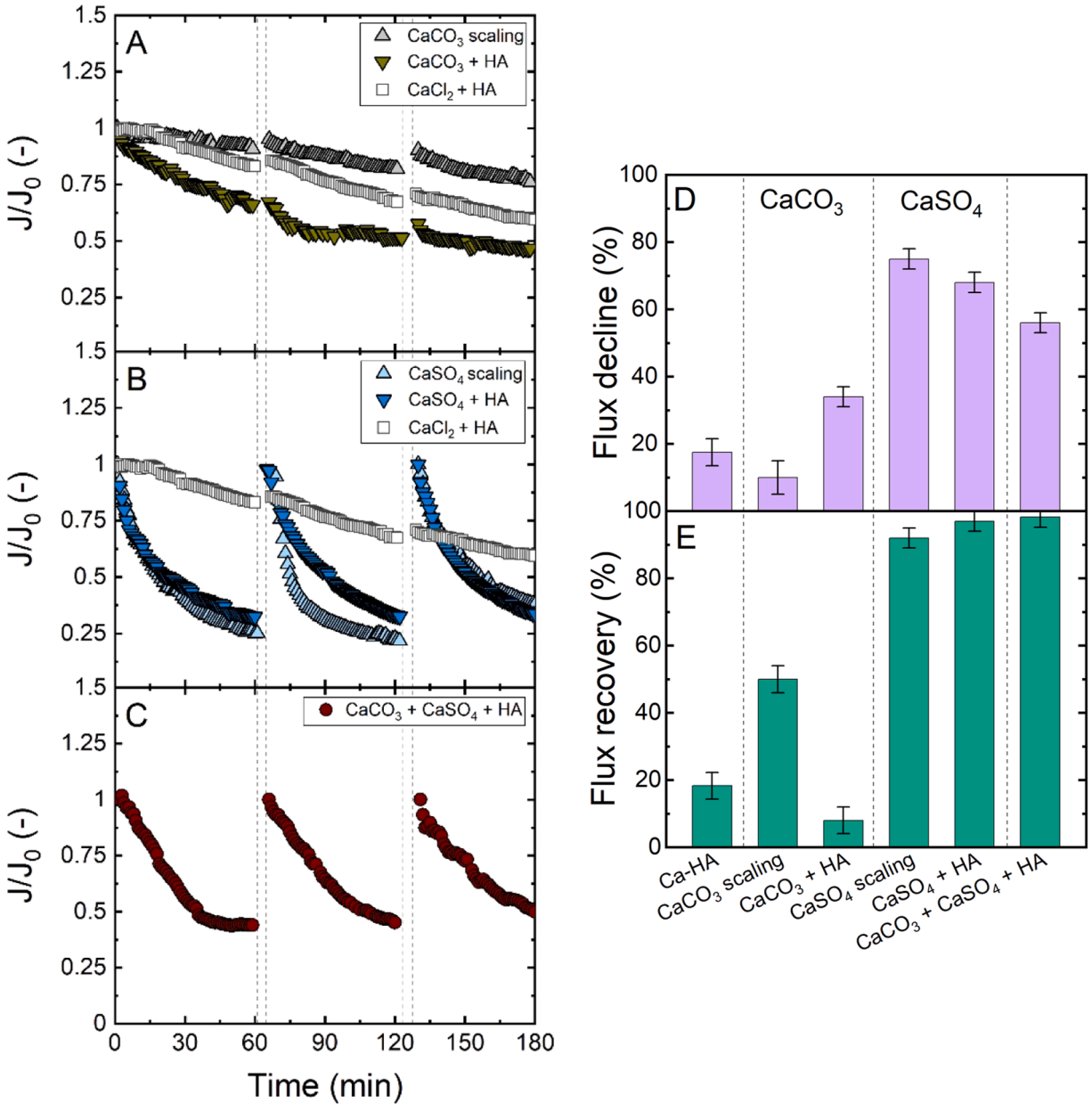

Fig. 10. Normalized flux observed for feed solutions with: (A) 4 mM $CaCO_3$ and 4 mM $CaCO_3$ + 5 mgC/L HA, (B) 25 mM $CaSO_4$, and 25 mM $CaSO_4$ + 5 mgC/L HA, (C) 4 mM $CaCO_3$ + 25 mM $CaSO_4$ + 5 mgC/L HA, and associated (D) flux decline and (E) flux recovery. (pH 8.0±0.1, 24±1 °C).

compared to $CaSO_4$ alone. When considering $CaCO_3$, greater flux decline with HA was likely due to increased material deposition on the membrane and a combination of scaling as well as fouling due to HA, which exhibits strong adhesion interactions with NF membranes (Cai et al., 2022b). At the comparatively high concentration of $CaSO_4$ (25 mM) vs. $CaCO_3$ (4 mM), fouling due to HA may have had a proportionally lower contribution to flux decline which was mainly due to increased CP driven by the greater mass deposition of $CaSO_4$ crystals that were readily released during OB. During filtration experiments with $CaCO_3$ + $CaSO_4$ + HA, substantial flux decline (~50%) was observed, however nearly 100% flux recovery was achieved during OB. Similar to observations for $CaSO_4$ + HA, flux decline was likely predominated by CP and scaling, which was readily released during OB. As such, with the exception of combined scaling and OM fouling for $CaCO_3$ + HA, the concentration of

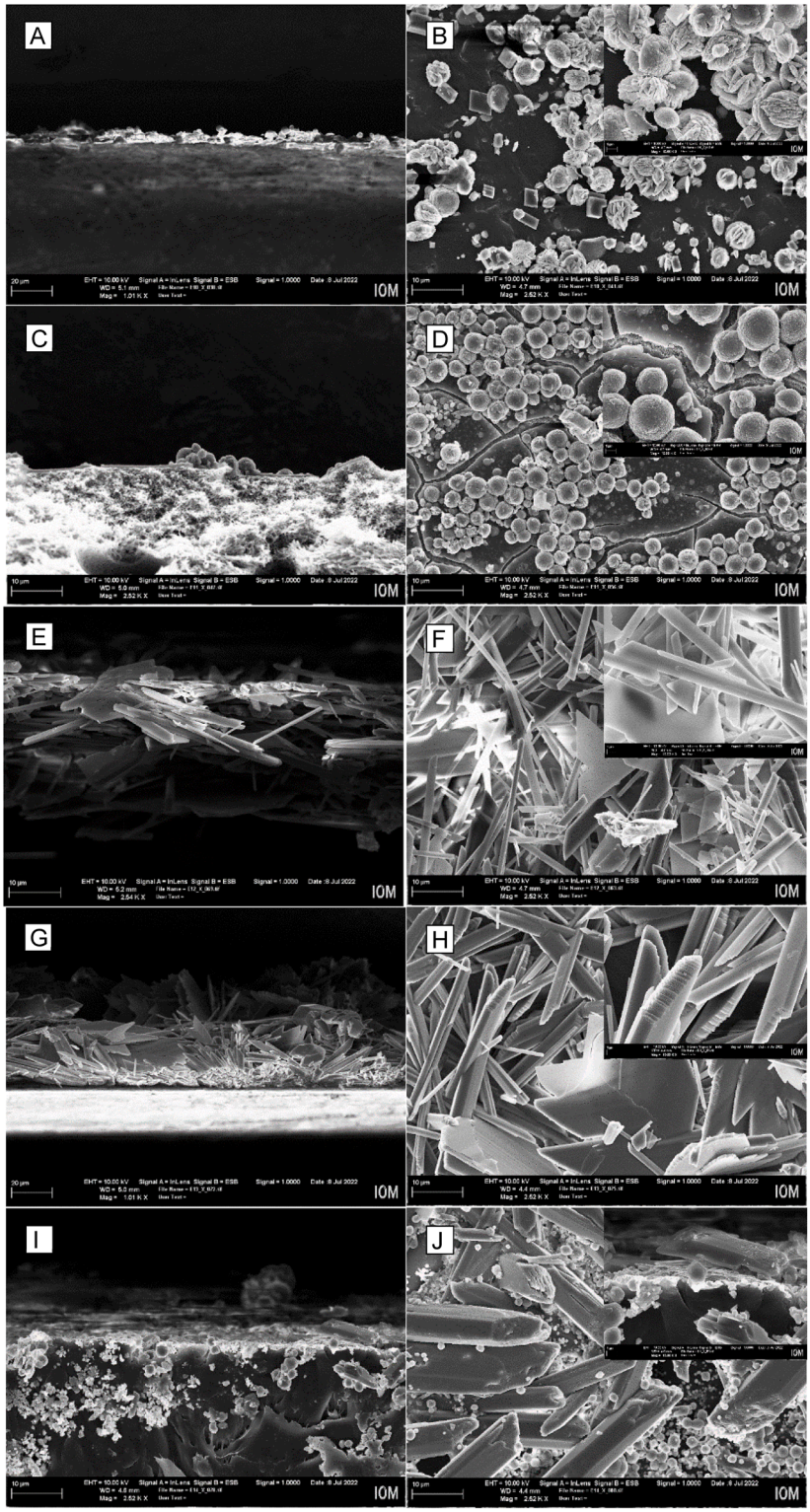

Fig. 11. Fouling layer thickness and structure on membrane samples for feed solutions with: (A-B) 4 mM $CaCO_3$, (C-D) 4 mM $CaCO_3$ + 5 mgC/L HA, (E-F) 25 mM $CaSO_4$, (G-H) 25 mM $CaSO_4$ + 5 mgC/L HA, and (I-J) 4 mM $CaCO_3$ + 25 mM $CaSO_4$ + 5 mgC/L HA. (pH 8.0±0.1, 24±1 °C).

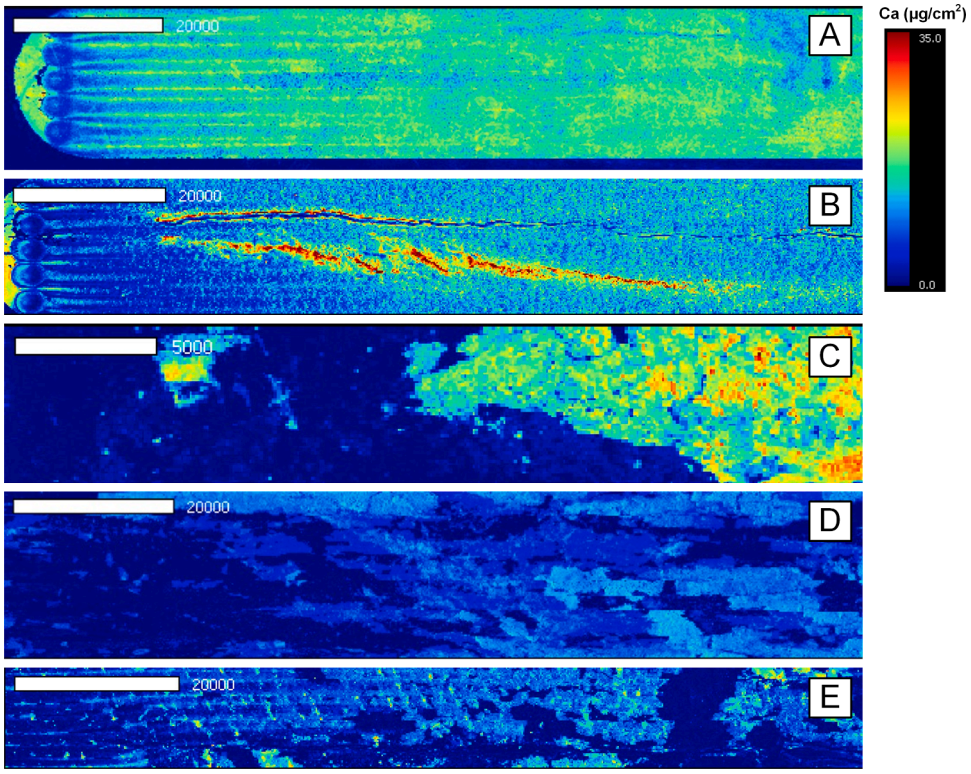

Fig. 12. Surface mapping of Ca deposition (0–35 μg/cm^2) within the fouling layer on membrane samples for feed solutions containing: (A) 4 mM $CaCO_3$, (B) 4 mM $CaCO_3$ + 5 mgC/L HA, (C) 25 mM $CaSO_4$, (D) 25 mM $CaSO_4$ + 5 mgC/L HA, and (E) 4 mM $CaCO_3$ + 25 mM $CaSO_4$ + 5 mgC/L HA. (pH 8.0±0.1, 24±1 °C).

HA (5 mgC/L) considered in the present study had a negligible contribution to membrane flux decline.

To investigate the contribution of Ca-OM enhanced fouling (Ca conditioning, Ca-OM aggregation) and scaling mechanisms to observed flux decline trends during filtration experiments, additional information is required regarding the characteristics of fouling layers present on membrane samples, which was discussed below.

3.7. Visualization of scalant-organic matter fouling layers

Fouling layers were qualitatively characterized in terms of structure and crystal morphology using FE-SEM (Fig. 11). Fouling layer characteristics for membrane samples obtained following filtration experiments where Ca and OM coexisted were compared to those of samples from filtration experiments with scalants alone. It was anticipated that the coexistence of $CaCO_3$ and $CaSO_4$ with HA would result in visible differences in crystal morphology.

Images of membrane samples obtained following filtration experiments with $CaCO_3$ alone show rhombohedral and spherical crystal morphologies characteristic of calcite and vaterite, respectively (Cherkas et al., 2018). Irregularities on the surface of vaterite crystals may indicate the occurrence of dissolution-recrystallization, which proceed calcite formation. In the presence of HA, a layer of OM fouling is visible beneath vaterite crystals, which likely reduced the permeability of the fouling layer and resulted in greater flux decline observed for HA with $CaCO_3$ when compared to $CaCO_3$ alone. When considering filtration experiments with $CaSO_4$, clusters of needle/rod- and plate-like gypsum crystals formed both with and without HA. However, the cross-sectional FE-SEM image shows evidence of rosette-like crystal morphology with HA, which indicates the occurrence of surface crystallization by heterogeneous nucleation (Boo et al., 2018). It has been suggested that HA fouling can enhance gypsum surface crystallization by providing nuclei for crystal growth (Wang et al., 2016).

For filtration experiments with $CaCO_3$ + $CaSO_4$ + HA, both rod-like gypsum and spherical vaterite crystals were visible within the fouling layer. Limited changes in crystal morphologies for membrane samples from filtration experiments conducted with versus without HA further suggest that the HA concentration considered did not substantially affect $CaCO_3$ or $CaSO_4$ crystallization.

While FE-SEM provided insight regarding crystal morphology attributed to specific scaling mechanisms, analysis of Ca deposition was performed to gain insight regarding the contribution of Ca to Ca-OM enhanced fouling and scaling mechanisms.

3.8. Spatial distribution of calcium deposits in scalant-organic matter fouling layers

To determine the role of Ca in Ca-enhanced OM fouling (Ca conditioning, Ca-OM aggregation) and scaling mechanisms, visualization of Ca deposition on membrane samples was obtained by surface mapping using μ-XRF (Fig. 12). Ca deposition was anticipated to be greatest for scaling as well as Ca-OM aggregation, which exhibited higher Ca deposition when compared to Ca conditioning during filtration experiments with different OM types.

Surface mapping results from XRF indicate that Ca deposition was highest for filtration experiments with $CaCO_3$ and $CaCO_3$ + HA. This correlated with lower flux recoveries following OB when compared to other experiments, and visual evidence of an OM fouling layer beneath $CaCO_3$ crystals. Ca deposition for the filtration experiments with $CaSO_4$ was comparatively low, which correlated with high flux recovery. High flux recovery was likely due to the formation of large crystals that produced a permeable fouling layer and were subjected to greater lift forces during OB when compared to smaller $CaCO_3$ crystals, which facilitated their release from the membrane surface. Similarly, filtration experiments with $CaCO_3$ + $CaSO_4$ + HA exhibited comparatively low Ca deposition; likely due to the formation of large crystals and a loose fouling layer that was readily released during OB.

To identify predominant Ca-enhanced OM fouling (Ca conditioning,

Ca-OM aggregation) and scaling mechanisms when scalants and OM coexist, additional information regarding Ca speciation within the fouling layer of membrane samples was required.

3.9. Calcium speciation in scalant-organic matter fouling layers

To reveal Ca speciation in the fouling layer of a membrane sample, a multi-energy (ME) map was generated using μ-XRF (4045.48, 4049.36, 4051.46, 4059.53 eV) and μ-XANES spectra were collected at 13 different locations (5 μm spot size) (Fig. 13). The membrane sample from the filtration experiment using $CaCO_3$ + $CaSO_4$ + HA was selected for this analysis as it was expected to contain different Ca species distinctive of i) Ca conditioning, ii) Ca-OM aggregation, and iii) scalant crystal types (calcite, vaterite, gypsum).

Normalized absorbance spectra from select spot locations on the membrane sample exhibit characteristic features associated with Ca conditioning and Ca-OM aggregation as well as different $CaCO_3$ and $CaSO_4$ crystal polymorphs, indicating that Ca-enhanced OM fouling and scaling mechanisms occurred simultaneously. $CaCO_3$ crystal polymorphs included vaterite, as was previously indicated from crystal morphology observed using FE-SEM, calcite, aragonite, and amorphous calcium carbonate (ACC). Normalized absorbance spectra from select spot locations exhibited high fraction values of gypsum (spots 5 and 7) as well as the membrane sample spectrum from the filtration experiment using $CaSO_4$ alone (spot 8), which may have included anhydrite and bassanite polymorphs, but this was not confirmed.

Membrane sample analysis using μ-XRF and μ-XANES was effective for identifying the simultaneous occurrence of Ca conditioning and Ca-OM aggregation mechanisms, while scaling mechanisms (bulk, surface crystallization) were not readily distinguishable. The potential to link the presence of specific crystal polymorphs with bulk and surface crystallization could be further explored using X-ray scattering techniques.

4. Conclusions

The objective of this research was to gain specific insight regarding Ca-enhanced OM fouling of NF membranes for a broad range of OM types, as well as Ca conditioning/Ca-OM aggregation fouling and scaling mechanisms when OM and scalants coexist using synchrotron-based μ-XRF and μ-XANES. Ca-OM aggregation dominates flux decline and decreases flux recovery following OB when compared to Ca conditioning (as defined in this study). OM types with both high density of carboxylic groups as well as negative charge exhibited a higher propensity for complexation with Ca. Surface mapping of membrane samples using XRF confirmed increased deposition of Ca on the membrane surface due to Ca-OM aggregation as a contributor to flux decline. LCF analysis of XANES spectra was able to reveal changes in the Ca coordination environment characteristic of Ca-OM aggregation for TEA, TA, and SA.

The coexistence of HA with $CaCO_3$ and $CaSO_4$ imparted negligible changes on Ca-enhanced OM fouling and scaling mechanisms for the feed solution compositions considered in the present study. For filtration of feed solution with $CaCO_3$ + $CaSO_4$ + HA, combined μ-XRF and μ-XANES analysis of the membrane sample effectively identified Ca speciation associated with Ca conditioning and Ca-OM aggregation mechanisms, as well as different $CaCO_3$ and $CaSO_4$ crystal polymorphs. The potential to link predominant crystal polymorphs with specific scaling mechanisms could enable the indirect identification of scaling mechanisms using μ-XRF and μ-XANES.

μ-XRF and XANES provide powerful tools for understanding membrane fouling mechanisms through the quantification of Ca deposition as well as identification of Ca speciation. μ-XRF and XANES are well suited for the investigation of membrane fouling mechanisms resulting from the filtration of feed solutions of different chemistries (e.g. inorganic, organic matter content) beyond those considered herein. By establishing a link between fouling mechanisms and membrane performance (e.g. flux decline and recovery), μ-XRF and XANES could enable the targeted

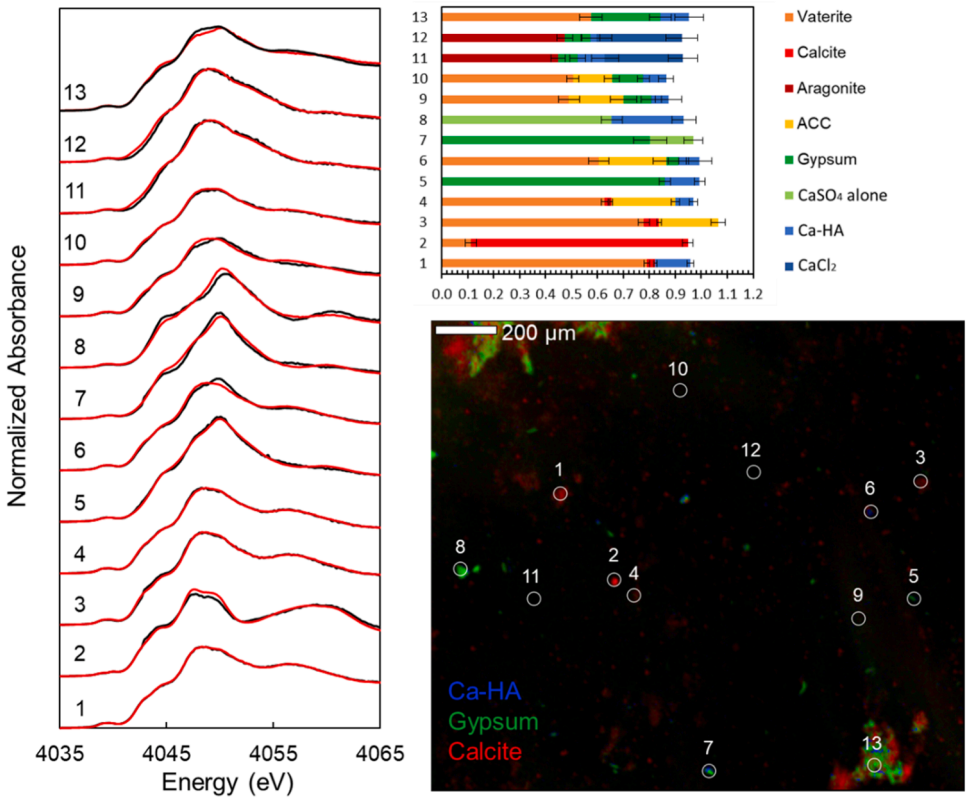

Fig. 13. Multi-energy (ME) map showing the spatial distribution of Ca speciation within the fouling layer on the membrane sample for $CaCO_3$ + $CaSO_4$ + HA. (4 mM $CaCO_3$ + 25 mM $CaSO_4$ + 5 mgC/L HA, pH 8.0±0.1, 24±1 °C).

selection of water treatment strategies to disrupt fouling mechanisms, as well as post-application evaluations of the degree to which fouling mechanisms are disrupted.

OM types with high carboxyl group density and negative charge should be targeted during pre-treatment to neutralize or eliminate (through removal) interactions with Ca. When considering the filtration of feed solutions containing Ca and different OM types, there were marked differences in OB efficiency (i.e. flux recovery) between OM types. For the coexistence of OM and scalants, OB efficiency was substantially higher for $CaSO_4$ when compared to $CaCO_3$ despite greater flux decline. Insight regarding the extent to which OM and scalant types affect OB efficiency could be used to screen its viability for fouling control based on source water characteristics.

CRediT authorship contribution statement

Tyler A. Malkoske: Writing – original draft, Writing – review & editing, Visualization, Validation, Formal analysis. **Yang-Hui Cai:** Writing – review & editing, Visualization, Validation, Methodology, Investigation, Formal analysis, Data curation, Conceptualization. **Sharon E. Bone:** Writing – review & editing, Visualization, Methodology, Investigation, Funding acquisition, Formal analysis, Data curation. **Andrea I. Schäfer:** Writing – review & editing, Supervision, Resources, Project administration, Funding acquisition, Conceptualization.

Declaration of competing interest

The authors declare that they have no known competing financial interests or personal relationships that could have appeared to influence the work reported in this paper.

Acknowledgements

Funding: The Helmholtz Association Recruitment Initiative and Helmholtz-ERC Recognition Award (HGF ERC-RA0032) are acknowledged for providing funding to IAMT-KIT. China Scholarship Council (CSC) granted a Ph.D. scholarship to Y.-H. Cai. This work was supported by the SLAC National Accelerator Laboratory Director's Fund. Use of the Stanford Synchrotron Radiation Lightsource, SLAC National Accelerator Laboratory, is supported by the U.S. Department of Energy, Office of Science, Office of Basic Energy Sciences under Contract No. DE-AC02-76SF00515.

The authors acknowledge Dr. Kristina Fischer (IOM) for providing FE-SEM images of membrane samples, Prof. Dr. Hans-Georg Steinrück (Forschungszentrum Jülich) for input on XANES methodology and data analysis, Dr. –Ing. Minh Nhat Nguyen (IAMT-KIT) for insight regarding OM surface chemistry and assistance with error analysis, and DuPont Water Solutions Co. for providing NF270 membranes.

Supplementary materials

The supporting information includes: (1) filtration experiment protocol, (2) error analysis, (3) quantification of organic matter deposition, (4) feed solution temperature and pH during filtration experiments, and (5) applied pressure and conductivity during filtration experiments, (6) TOC deposition for bridging and complexation experiments, and (7) XANES reference spectra for LCF. Supplementary material associated with this article can be found, in the online version, at doi:10.1016/j.watres.2024.122938.

Data availability

Data will be made available on request.

References

Adams, F., 2010. Synchrotron X-ray fluorescence analysis in environmental and earth sciences. EPJ Web Conf. 9, 165–180.
Adusei-Gyamfi, J., Ouddane, B., Rietveld, L., Cornard, J.-P., Criquet, J., 2019. Natural organic matter-cations complexation and its impact on water treatment: a critical review. Water Res. 160, 130–147.
Al Haj, R., Merheb, M., Halwani, J., Ouddane, B, 2023. Hydrogeochemical characteristics of groundwater in the Mediterranean region: a meta-analysis. Phys. Chem. Earth, Parts A/B/C 129, 103351.
Alnumani, A., Matin, A., Farooque, M., Green, T., Falath, W., Aljundi, I., Khalifa, A., Rahman, M., Laoui, T., Abutaleb, A., 2024. Osmotic-induced cleaning is effective in long-term fouling mitigation of reverse osmosis elements at pilot plant level. Desalination 578, 117336.
Antony, A., Low, J.H., Gray, S., Childress, A.E., Le-Clech, P., Leslie, G., 2011. Scale formation and control in high pressure membrane water treatment systems: a review. J. Membr. Sci. 383 (1-2), 1–16.
Barry, M.E., Landsman, M.R., Nomaan, S.M., Gokturk, P.A., Cooper, C.M., Kienzle, B.A., McKay, C., Katz, L.E., 2020. Expanding the use of synchrotron techniques for water treatment: from minerals to membranes. Synchrotron Radiat. News 33 (4), 3–12.
Benecke, J., Rozova, J., Ernst, M., 2018. Anti-scale effects of select organic macromolecules on gypsum bulk and surface crystallization during reverse osmosis desalination. Sep. Purif. Technol. 198, 68–78.
Bone, S.E., Steinrück, H.-G., Toney, M.F., 2020. Advanced characterization in clean water technologies. Joule 4 (8), 1637–1659.
Boo, C., Wang, Y., Zucker, I., Choo, Y., Osuji, C.O., Elimelech, M., 2018. High performance nanofiltration membrane for effective removal of perfluoroalkyl substances at high water recovery. Environ. Sci. Technol. 52 (13), 7279–7288.
Boussu, K., De Baerdemaeker, J., Dauwe, C., Weber, M., Lynn, K.G., Depla, D., Aldea, S., Vankelecom, I.F.J., Vandecasteele, C., Van der Bruggen, B., 2007. Physico-chemical characterization of nanofiltration membranes. Chemphyschem 8 (3), 370–379.
Cai, Y.-H., Boussouga, Y.-A., Schäfer, A.I., 2024. Renewable energy powered membrane technology: impact of intermittency on membrane integrity. Desalination 580, 117504.
Cai, Y.-H., Burkhardt, C.J., Schäfer, A.I., 2021. Renewable energy powered membrane technology: impact of osmotic backwash on scaling during solar irradiance fluctuation. J. Membr. Sci. 619, 118799.
Cai, Y.-H., Burkhardt, C.J., Schäfer, A.I., 2022a. Renewable energy powered membrane technology: impact of osmotic backwash on organic fouling during solar irradiance fluctuation. J. Membr. Sci. 647, 120286.
Cai, Y.-H., Schäfer, A.I., 2020. Renewable energy powered membrane technology: impact of solar irradiance fluctuation on direct osmotic backwash. J. Membr. Sci. 598, 117666.
Cai, Y.H., Gopalakrishnan, A., Deshmukh, K.P., Schäfer, A.I., 2022b. Renewable energy powered membrane technology: implications of adhesive interaction between membrane and organic matter on spontaneous osmotic backwash cleaning. Water Res. 221, 118752.
Calvin, S., 2013. XAFS for Everyone. Taylor & Francis.
Cao, T., Rolf, J., Wang, Z., Violet, C., Elimelech, M., 2022. Distinct impacts of natural organic matter and colloidal particles on gypsum crystallization. Water Res. 218, 118500.
Cherkas, O., Beuvier, T., Zontone, F., Chushkin, Y., Demoulin, L., Rousseau, A., Gibaud, A., 2018. On the kinetics of phase transformations of dried porous vaterite particles immersed in deionized and tap water. Adv. Powder Technol. 29 (11), 2872–2880.
Chon, K., Cho, J., 2016. Fouling behavior of dissolved organic matter in nanofiltration membranes from a pilot-scale drinking water treatment plant: An autopsy study. J. Chem. Eng. 295, 268–277.
Chong, T.H., Sheikholeslami, R., 2001. Thermodynamics and kinetics for mixed calcium carbonate and calcium sulfate precipitation. Chem. Eng. Sci. 56 (18), 5391–5400.
Curcio, E., Ji, X., Di Profio, G., Sulaiman, A.O., Fontananova, E., Drioli, E., 2010. Membrane distillation operated at high seawater concentration factors: role of the membrane on $CaCO_3$ scaling in presence of humic acid. J. Membr. Sci. 346 (2), 263–269.
Dydo, P., Turek, M., Ciba, J., 2003. Scaling analysis of nanofiltration systems fed with saturated calcium sulfate solutions in the presence of carbonate ions. Desalination 159 (3), 245–251.
Farfan, G.A., Apprill, A., Webb, S.M., Hansel, C.M., 2018. Coupled X-ray fluorescence and X-ray absorption spectroscopy for microscale imaging and identification of sulfur species within tissues and skeletons of scleractinian corals. Anal. Chem. 90 (21), 12559–12566.
Greenlee, L.F., Lawler, D.F., Freeman, B.D., Marrot, B., Moulin, P., 2009. Reverse osmosis desalination: water sources, technology, and today's challenges. Water Res. 43 (9), 2317–2348.
Helmiyati, Aprilliza, M, 2017. Characterization and properties of sodium alginate from brown algae used as an ecofriendly superabsorbent. IOP Conf. Ser.: Mater. Sci. Eng. 188, 012019.
Henderson, G.S., de Groot, F.M.F., Moulton, B.J.A., 2014. X-ray absorption near-edge structure (XANES) spectroscopy. Rev. Mineral. Geochem. 78 (1), 75–138.
Hong, S., Elimelech, M., 1997. Chemical and physical aspects of natural organic matter (NOM) fouling of nanofiltration membranes. J. Membr. Sci. 132, 159–181.
Hou, L.-B., Catherine, H.N., Harada, K., Yoshida, M., Chen, Y.-L., Hu, C., 2023. Reactive seeding growth of cobalt-doped MIL-88B(Fe) on Al_2O_3 membrane for phenol removal in a photocatalytic membrane reactor. J. Membr. Sci. 680, 121730.

Idil Mouhoumed, E., Szymczyk, A., Schäfer, A., Paugam, L., La, Y.H., 2014. Physico-chemical characterization of polyamide NF/RO membranes: insight from streaming current measurements. J. Membr. Sci. 461, 130–138.
Imbrogno, A., Tiraferri, A., Abbenante, S., Weyand, S., Schwaiger, R., Luxbacher, T., Schäfer, A.I., 2018. Organic fouling control through magnetic ion exchange-nanofiltration (MIEX-NF) in water treatment. J. Membr. Sci. 549, 474–485.
Iskrenova-Tchoukova, E., Kalinichev, A.G., Kirkpatrick, R.J., 2010. Metal cation complexation with natural organic matter in aqueous solutions: molecular dynamics simulations and potentials of mean force. Langmuir 26 (20), 15909–15919.
Karabelas, A., Karanasiou, A., Mitrouli, S., 2014. Incipient membrane scaling by calcium sulfate during desalination in narrow spacer-filled channels. Desalination 345, 146–157.
Khasnabis, J., Rai, C., Roy, A., 2015. Determination of tannin content by titrimetric method from different types of tea. J. Chem. Pharm. Res. 7 (8), 238–241.
Kum, S., Landsman, M.R., Su, G.M., Freychet, G., Lawler, D.F., Katz, L.E., 2021. Performance of a hybrid ED–NF membrane system for water recovery improvement via NOM fouling control. ACS ES&T Eng. 1 (10), 1420–1431.
Lee, H., Im, S.-J., Lee, H., Kim, C.-M., Jang, A., 2021. Comparative analysis of salt cleaning and osmotic backwash on calcium-bridged organic fouling in nanofiltration process. Desalination 507, 115022.
Lee, S., Elimelech, M., 2006. Relating organic fouling of reverse osmosis membranes to intermolecular adhesion forces. Environ. Sci. Technol. 40 (3), 980–987.
Li, D., Yang, X., Zhou, Z., Jiang, B., Tawfik, A., Zhao, S., Meng, F., 2019. Molecular traits of phenolic moieties in dissolved organic matter: linkages with membrane fouling development. Environ. Int. 133, 105202.
Li, Q., Elimelech, M., 2004. Organic fouling and chemical cleaning of nanofiltration membranes: measurements and mechanisms. Environ. Sci. Technol. 38, 4683–4693.
Li, W., Liu, X., Wang, Y.-N., Chong, T.H., Tang, C.Y., Fane, A.G., 2016. Analyzing the evolution of membrane fouling via a novel method based on 3D optical coherence tomography imaging. Environ. Sci. Technol. 50 (13), 6930–6939.
Lin, D., Bai, L., Xu, D., Wang, H., Zhang, H., Li, G., Liang, H., 2021. Nanofiltration scaling influenced by coexisting pollutants considering the interaction between ferric coagulant and natural organic macromolecules. Chem. Eng. J. 413, 127403.
Lipczynska-Kochany, E., 2018. Effect of climate change on humic substances and associated impacts on the quality of surface water and groundwater: a review. Sci. Total Environ. 640-641, 1548–1565.
López-Muñoz, M.J., Sotto, A., Arsuaga, J.M., Van der Bruggen, B., 2009. Influence of membrane, solute and solution properties on the retention of phenolic compounds in aqueous solution by nanofiltration membranes. Sep. Purif. Technol. 66 (1), 194–201.
Martin-Diaconescu, V., Gennari, M., Gerey, B., Tsui, E., Kanady, J., Tran, R., Pécaut, J., Maganas, D., Krewald, V., Gouré, E., Duboc, C., Yano, J., Agapie, T., Collomb, M.-N., DeBeer, S., 2015. Ca K-edge XAS as a probe of calcium centers in complex systems. Inorg. Chem. 54 (4), 1283–1292.
Mewes, A., Langer, G., de Nooijer, L.J., Bijma, J., Reichart, G.-J., 2014. Effect of different seawater Mg^{2+} concentrations on calcification in two benthic foraminifers. Mar. Micropaleontol. 113, 56–64.
Mi, B., Elimelech, M., 2008. Chemical and physical aspects of organic fouling of forward osmosis membranes. J. Membr. Sci. 320 (1), 292–302.
Mi, B., Elimelech, M., 2010. Gypsum scaling and cleaning in forward osmosis: measurements and mechanisms. Environ. Sci. Technol. 44 (6), 2022–2028.
Mitchell, G.E., Mickols, B., Hernandez-Cruz, D., Hitchcock, A., 2011. Unexpected new phase detected in FT30 type reverse osmosis membranes using scanning transmission X-ray microscopy. Polymer 52 (18), 3956–3962.
Nguyen, M.N., Hérvas-Martínez, R., Schäfer, A.I., 2021. Organic matter interference with steroid hormone removal by single-walled carbon nanotubes – ultrafiltration composite membrane. Water Res. 199, 117148.
Niemann, V.A., Huck, M., Steinrück, H.-G., Toney, M.F., Tarpeh, W.A., Bone, S.E., 2023. X-ray absorption spectroscopy reveals mechanisms of calcium and silicon fouling on reverse osmosis membranes used in wastewater reclamation. ACS ES. T. Water. 3 (8), 2627–2637.
Park, J., Lee, S., You, J., Park, S., Ahn, Y., Jung, W., Cho, K.H., 2018. Evaluation of fouling in nanofiltration for desalination using a resistance-in-series model and optical coherence tomography. Sci. Total Environ. 642, 349–355.
Park, S., Saavedra, M., Liu, X., Li, T., Anger, B., Tong, T., 2024. A comprehensive study on combined organic fouling and gypsum scaling in reverse osmosis: decoupling surface and bulk phenomena. J. Membr. Sci. 694, 122399.
Pignon, F., Abyan, M., David, C., Magnin, A., Sztucki, M., 2012. In situ characterization by SAXS of concentration polarization layers during cross-flow ultrafiltration of Laponite dispersions. Langmuir 28 (2), 1083–1094.
Prietzel, J., Klysubun, W., Hurtarte, L.C.C., 2021. The fate of calcium in temperate forest soils: a Ca K-edge XANES study. Biogeochemistry 152 (2), 195–222.
Quay, A.N., Tong, T., Hashmi, S.M., Zhou, Y., Zhao, S., Elimelech, M., 2018. Combined organic fouling and inorganic scaling in reverse osmosis: role of protein–silica interactions. Environ. Sci. Technol. 52 (16), 9145–9153.
Ravel, B., Newville, M., 2005. Athena, Artemis, Hephaestus: data analysis for X-ray absorption spectroscopy using IFEFFIT. J. Synchrotron Rad. 12, 537–541.
Rolf, J., Cao, T., Huang, X., Boo, C., Li, Q., Elimelech, M., 2022. Inorganic scaling in membrane desalination: models, mechanisms, and characterization methods. Environ. Sci. Technol. 56 (12), 7484–7511.
Rowley, M.C., Nico, P.S., Bone, S.E., Marcus, M.A., Pegoraro, E.F., Castanha, C., Kang, K., Bhattacharyya, A., Torn, M.S., Peña, J., 2023. Association between soil organic carbon and calcium in acidic grassland soils from Point Reyes National Seashore. CA Biogeochemistry 165 (1), 91–111.
Ruiz-García, A., Melián-Martel, N., Mena, V., 2018. Fouling characterization of RO membranes after 11years of operation in a brackish water desalination plant. Desalination 430, 180–185.
Sagiv, A., Semiat, R., 2005. Backwash of RO spiral wound membranes. Desalination 179, 1–9.
Sari, M.A., Chellam, S., 2017. Relative contributions of organic and inorganic fouling during nanofiltration of inland brackish surface water. J. Membr. Sci. 523, 68–76.
Schäfer, A.I., Andritsos, N., Karabelas, A.J., Hoek, E.M.V., Schneider, R., Nyström, M., 2021. In: Schäfer, A.I., Fane, A.G. (Eds.), Nanofiltration: Principles, Applications, and New Materials. Wiley-VCH GmbH, pp. 275–382.
Schäfer, A.I., Fane, A.G., Waite, T.D., 1998. Nanofiltration of natural organic matter: removal, fouling and the influence of multivalent ions. Desalination 118 (1), 109–122.
Schäfer, A.I., Hughes, G., Richards, B.S., 2014. Renewable energy powered membrane technology: a leapfrog approach to rural water treatment in developing countries? Renew. Sustain. Energy Rev. 40, 542–556.
Shim, Y., Lee, H.-J., Lee, S., Moon, S.-H., Cho, J., 2002. Effects of natural organic matter and ionic species on membrane surface charge. Environ. Sci. Technol. 36 (17), 3864–3871.
Singh, P.S., Ray, P., Xie, Z., Hoang, M., 2012. Synchrotron SAXS to probe cross-linked network of polyamide 'reverse osmosis' and 'nanofiltration' membranes. J. Membr. Sci. 421-422, 51–59.
Sowrey, F.E., Skipper, L.J., Pickup, D.M., Drake, K.O., Lin, Z., Smith, M.E., Newport, R.J., 2004. Systematic empirical analysis of calcium–oxygen coordination environment by calcium K-edge XANES. Phys. Chem. Chem. Phys. 6 (1), 188–192.
Tang, C.Y., Kwon, Y.-N., Leckie, J.O., 2007a. Characterization of humic acid fouled reverse osmosis and nanofiltration membranes by transmission electron microscopy and streaming potential measurements. Environ. Sci. Technol. 41 (3), 942–949.
Tang, C.Y., Kwon, Y.-N., Leckie, J.O., 2007b. Fouling of reverse osmosis and nanofiltration membranes by humic acid—effects of solution composition and hydrodynamic conditions. J. Membr. Sci. 290 (1), 86–94.
Tong, T., Liu, X., Li, T., Park, S., Anger, B., 2023. A tale of two foulants: the coupling of organic fouling and mineral scaling in membrane desalination. Environ. Sci. Technol. 57 (18), 7129–7149.
Vivar, M., H, S., Fuentes, M, 2024. Photovoltaic system adoption in water related technologies – a review. Renew. Sustain. Energy Rev. 189, 114004.
Wang, J., Wang, L., Miao, R., Lv, Y., Wang, X., Meng, X., Yang, R., Zhang, X., 2016. Enhanced gypsum scaling by organic fouling layer on nanofiltration membrane: characteristics and mechanisms. Water Res. 91, 203–213.
Webb, S.M., 2011. The MicroAnalysis toolkit: X-ray fluorescence image processing software. AIP Conf. Proc. 1365 (1), 196–199.
Willmott, P., 2019. An Introduction to Synchrotron radiation: Techniques and Applications. John Wiley & Sons.
Xie, M., Gray, S.R., 2016. Gypsum scaling in forward osmosis: role of membrane surface chemistry. J. Membr. Sci. 513, 250–259.
Yoon, S.-H., Lee, C.-H., Kim, K.-J., Fane, A.G., 1998. Effect of calcium ion on the fouling of nanofilter by humic acid in drinking water production. Water Res. 32 (7), 2180–2186.
Zheng, L., Zhong, H., Wang, Y., Duan, N., Ulbricht, M., Wu, Q., Van der Bruggen, B., Wei, Y., 2024. Mixed scaling patterns and mechanisms of high-pressure nanofiltration in hypersaline wastewater desalination. Water Res. 250, 121023.